



FIBER VOLUME FRACTION EFFECTS ON FATIGUE  
RESPONSE OF A SCS-6/Ti-15-3 METAL MATRIX  
COMPOSITE AT ELEVATED TEMPERATURE

THESIS

SEAN C. COGHLAN  
DAGSI  
AFIT/GAE/ENY/97S-01

**DISTRIBUTION STATEMENT A**

Approved for public release,  
Distribution Unlimited

DEPARTMENT OF THE AIR FORCE  
AIR UNIVERSITY  
**AIR FORCE INSTITUTE OF TECHNOLOGY**

Wright-Patterson Air Force Base, Ohio

DTIC QUALITY INSPECTED 4

AFIT/GAE/ENY/97S-01

FIBER VOLUME FRACTION EFFECTS ON FATIGUE  
RESPONSE OF A SCS-6/Ti-15-3 METAL MATRIX  
COMPOSITE AT ELEVATED TEMPERATURE

THESIS

SEAN C. COGHLAN  
DAGSI  
AFIT/GAE/ENY/97S-01

19970929 059

The views expressed in this thesis are those of the author and do not  
reflect the official policy or position of the Department of Defense  
or the U.S. Government.

Approved for public release; distribution unlimited

AFIT/GAE/ENY/97S-01

Fiber Volume Fraction Effects on Fatigue  
Response of a SCS-6/Ti-15-3 Metal Matrix  
Composite at Elevated Temperature

THESIS

Presented to the Faculty of the School of Engineering  
of the Air Force Institute of Technology  
Air University  
In Partial Fulfillment of the  
Requirements for the Degree of  
Master of Science in Aeronautical Engineering

Sean C. Coghlan

DAGSI

September 1997

Approved for public release; distribution unlimited

FIBER VOLUME FRACTION EFFECTS ON FATIGUE  
RESPONSE OF A SCS-6/Ti-15-3 METAL MATRIX  
COMPOSITE AT ELEVATED TEMPERATURE

SEAN C. COGHLAN  
DAGSI

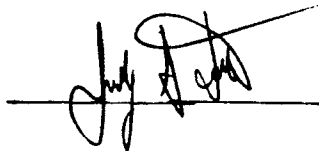
Approved:

  
Chairman

9/15/97  
date

  
W. Jerry Bouman

15 Sept 1997  
date

  
J. J. D. [unclear]

19 Sep 97  
date

## **Acknowledgments**

This project is successful only through the culmination of effort of several people. I would like to thank them for their assistance and knowledge here.

Dr. Shankar Mall, my advisor, for providing direction and demanding the effort required to achieve. His guidance will never be forgotten.

All of the programs used to perform this study were designed and written by Mark Derriso, to whom I am greatly thankful for. Every time my progress was stalled, he was there to solve any problem before going back to doing more important things. He and the rest of the laboratory staff; Andy Pitts, Dan Rioux, Charlie McNeely, and Jay Anderson kept me focused and thoroughly entertained during my work. I appreciate all their efforts in finding equipment, and providing professional advice. Dr. Jeff Calcaterra also gave a large amount of time to discussion of the finer points of MMC fatigue and college sports.

NASA Lewis Research Center was the project sponsor with Mike Castelli and Brad Lerch as the contacts. They provided the test material as well as insight on where the research should focus.

Machining support was provided by the great guys “down at the shop”. I extend a great amount of gratitude to Jack Tiffany, Mike and Jan.

Finally, I would like to acknowledge the Dayton Area Graduate Studies Institute (DAGSI) for providing this research opportunity that would not otherwise have been available.

## Table of Contents

Acknowledgments.....	ii
List of Figures.....	v
List of Tables.....	viii
Abstract.....	ix
1. Introduction.....	1
2. Background.....	5
2.1 Tension-Tension Fatigue .....	5
2.1.1 Load Control Mode.....	6
2.1.2 Strain Control Mode.....	8
2.2 Tension-Compression Fatigue.....	9
2.2.1 Load Control Mode.....	9
2.2.2 Strain Control Mode.....	11
3. Experiments.....	13
3.1 Material Description.....	13
3.2 Specimen Design and Preparation.....	15
3.3 Buckling Guide Description.....	17
3.4 Test Setup.....	18
3.5 Tests.....	21
3.6 Post Failure Analysis.....	22
4. Results and Discussion.....	24
4.1 Macro-mechanical Analysis.....	24
4.1.1 Consolidated Neat Matrix.....	25
4.1.2 15% Fiber Volume Fraction.....	26
4.1.3 25% Fiber Volume Fraction.....	34
4.1.4 42% Fiber Volume Fraction.....	38
4.1.5 Summary.....	41
4.2 Fatigue Life.....	42
4.2.1 Stress Control and Strain Control Comparison.....	45
4.2.2 Fiber Stress Analysis.....	50
4.3 Microscopic Analysis.....	52
4.3.1 15% Fiber Volume Fraction.....	52

4.3.2 25% Fiber Volume Fraction.....	59
4.3.3 42% Fiber Volume Fraction.....	66
5. Summary and Conclusions.....	71
Bibliography.....	75
Appendix: Stress-strain Loops.....	78
Vita.....	82

## List of Figures

1. Tension-Compression Wave Form.....	3
2. Three Regimes of Fatigue for SCS-6/Ti-15-3.....	7
3. $[0]_8$ Tension-Compression Fatigue Life Curve at 427°C.....	10
4. Schematic of Unidirectional $[0^\circ]$ Specimen Orientation.....	14
5. Dogbone Specimen Geometry for This Study.....	16
6. AFIT Buckling Guide used for this study.....	19
7. Test Apparatus.....	20
8. Location of Sections for Specimen Analysis.....	23
9. Definition of Different Moduli from a Stress-Strain Curve.....	25
10. Secant Modulus History of Neat Matrix.....	26
11. $\epsilon_{\max}=0.25\%$ ; Tensile and Compressive Modulus History.....	28
12. Secant Modulus Histories for 15% $V_f$ Tests.....	30
13. Modified Secant Modulus for 0.3% Test.....	31
14. Stress-strain Loops for 0.4% Maximum Strain Test.....	32
15. Stress-strain Loops for 0.003 mm/mm Test.....	33
16. Tensile Modulus Histories for 25% $V_f$ Tests.....	35
17. Modified Secant Modulus of the 0.3% Test.....	36
18. Stress-strain Loops for 0.4% Maximum Strain Test.....	37
19. Tensile Modulus Histories for the 42% $V_f$ Tests.....	39
20. Stress-strain Loops for 0.4% Maximum Strain Test.....	40



21. Moduli for 0.3% Strain Tests for all $V_f$ .....	41
22. S-N Diagram for 42% and 36% $V_f$ .....	43
23. S-N Diagram for 15%, 36%, and 42% $V_f$ .....	43
24. S-N Diagram for all Fiber Volume Fractions.....	44
25. S-N Diagram for High $V_f$ Under Stress and Strain Control.....	46
26. S-N Diagram for all data except 25% $V_f$ .....	47
27. S-N Diagram for all $V_f$ and Control Modes.....	47
28. S-N Diagram for 15% $V_f$ Stress and Strain Control.....	49
29. Fiber Stress Range versus Cycles for all Fiber Volume Fractions.....	51
30. Molybdenum Cross-Weave on the Fracture Surface.....	53
31. 0.0025 mm/mm 15% $V_f$ Specimen Fracture Surface.....	54
32. 0.0055 mm/mm 15% $V_f$ Specimen Fracture Surface.....	55
33. 0.0035 mm/mm 15% $V_f$ Specimen Fracture Surface.....	55
34. Ductile Rupture Matrix Dimples.....	56
35. 0.0035 mm/mm 15% $V_f$ Specimen Fracture Surface.....	57
36. 0.0055 mm/mm Specimen Face Away From Fracture Surface.....	58
37. Large Dimples on Matrix/Matrix Interface.....	59
38. 0.003 mm/mm 25% $V_f$ Specimen Fracture Surface.....	60
39. 0.004 mm/mm 25% $V_f$ Specimen Fracture Surface.....	61
40. Side View of 0.004 mm/mm 25% $V_f$ Specimen.....	62
41. 0.0035 mm/mm 25% $V_f$ Specimen Fracture Surface.....	62

42. Fractured Fibers Ahead of the Crack Tip (5x).....	63
43. Matrix Crack on Specimen Edge, 0.8% Strain Range (5x).....	64
44. Fiber Bridged Matrix Crack (40x).....	65
45. Undamaged Specimen Face in Gage Length, 0.7% Strain (5x).....	65
46. 0.004 mm/mm Specimen Fracture Surface.....	66
47. 0.003 mm/mm Specimen Fracture Surface.....	67
48. 0.0035 mm/mm Specimen Fracture Surface.....	67
49. Damage Initiated From Mo Cross-Weave (10x).....	69
50. Fiber/Matrix Interface Damage at Mo Cross-Weave (100x).....	69

## **List of Tables**

1. Fiber and Matrix Properties.....	14
2. Test Matrix.....	22
3. 15% $V_f$ TMC Test Matrix.....	27
4. 25% $V_f$ TMC Test Matrix.....	35
5. 42% $V_f$ TMC Test Matrix.....	38

## Abstract

The purpose of this study was to determine the effects of fiber volume fraction on the fatigue behavior of Silicon Carbide fiber-reinforced Titanium alloy, SCS-6/Ti-15-3. Three fiber volume fractions were investigated; 15%, 25%, and 42%. The tests were performed under fully-reversed, strain-controlled conditions at 427°C. The primary objectives of this study were to develop a fatigue life diagram and to document the damage and failure mechanisms.

Compressive loads on the slender specimens were kept from buckling the specimens through the use of a buckling guide. This device allows unrestricted axial movement of the composite, while preventing any out-of-plane motion. No buckling damage due to compression was found in any of the specimens.

Modulus behavior and stress versus strain curves were recorded during cycling for each test. An applied strain range between 0.5% and 1.1% was used for the majority of the tests. This resulted in fatigue lives between approximately 10,000 and 100,000 cycles. The resulting fatigue life diagram showed similar life at strain ranges at and above 0.008 mm/mm for all fiber volume fractions. At strain levels below 0.008 mm/mm, there was an increasing fatigue life with increasing fiber volume fraction.

The 15% and 42%  $V_f$  material was consolidated with a molybdenum cross-weave to hold the fibers in alignment. The 25%  $V_f$  material had a titanium-niobium cross-weave for the same purpose. The Mo cross-weave was present on every fracture surface of the 15% and 42%  $V_f$  material. This indicated that it was detrimental to the fatigue life of the composite. No cross-weave material was found on the fracture surfaces of the 25%  $V_f$ .

Major cause of specimen failure was the initiation and propagation of fatigue cracks in the matrix that were perpendicular to the applied load. Once the cracks had grown large enough, the specimens failed in tensile overload. Only one high applied strain range test exhibited fiber breakage away from the fracture surface.

# **FIBER VOLUME FRACTION EFFECTS ON FATIGUE RESPONSE OF A SCS-6/Ti-15-3 METAL MATRIX COMPOSITE AT ELEVATED TEMPERATURE**

## **1. Introduction**

The need to satisfy higher performance programs such as the Integrated High Performance Turbine Engine Technology (IHPTET) and the High Speed Civil Transport (HSCT) has stimulated recent development of Metal Matrix Composites (MMCs). These MMCs offer high stiffness and strength to weight ratios, better toughness than ceramic matrix composites, and good elevated temperature properties.

One class of MMCs uses titanium alloy with silicon carbide reinforcing fibers. These Titanium Matrix Composites (TMCs) have high modulus, impact, and temperature properties. To be economically feasible, an extended service life is desired from these materials. Since engine components experience repeated mechanical and thermal loads, application of TMCs into these components requires an intensive investigation into their fatigue properties. To date, many studies have investigated tension-tension or zero-tension fatigue behavior of TMCs in elevated or room temperature isothermal conditions [5,7,9,10,11,12,15,22,23,28]. Many different composite lay-ups of TMCs have been tested including off-axis plies which have been shown to reduce the strength of the composite [15,19,28]. These off-axis plies are layers in the laminate where the silicon carbide fibers are not aligned with the applied load. Engine components are also subjected to Thermo-Mechanical Fatigue (TMF), where both temperature and load are applied cyclically. Several studies have investigated this type of fatigue which have been shown to significantly reduce the fatigue life of TMC [5,6,10,21].

Even with all the material characterization as briefly discussed above, there are still areas that need to be investigated before TMCs can be employed in engine components efficiently. The majority of previous studies were performed under load control mode and used a material with a fiber volume fraction ( $V_f$ ) of 35%. Previous studies have shown that the fiber/matrix interfacial zone in TMCs is one of the problems during fatigue loading [16,20]. Laminates will have different interfacial area with varying  $V_f$  and its effect on fatigue life must be examined. Therefore  $V_f$ 's of other than 35% should be studied for comparison.

Typical low cycle fatigue testing of monolithic alloys is done under strain control mode [18]. Load controlled low cycle fatigue tests of monolithics lead to unconstrained ratchetting and localized necking. These mechanisms are unlike the fatigue cracking mechanism being studied in the present study and also highly undesirable [18]. Further, testing of TMCs under fully-reversed, elevated-temperature, strain-controlled conditions has not been well covered.

The purpose of this study was therefore to investigate the fatigue behavior of a unidirectional TMC laminate with three different fiber volume fractions under fully-reversed, strain-controlled conditions at 427°C. The TMC chosen was SCS-6/Ti-15-3, which is a metastable titanium beta alloy matrix, Ti-15-3, reinforced with silicon carbide fibers, SCS-6. In this study, several tests were conducted at a strain ratio,  $R = -1.0$ . All tests were run at a constant strain rate of 0.001 mm/mm/s with the triangular waveform shown in Figure 1.

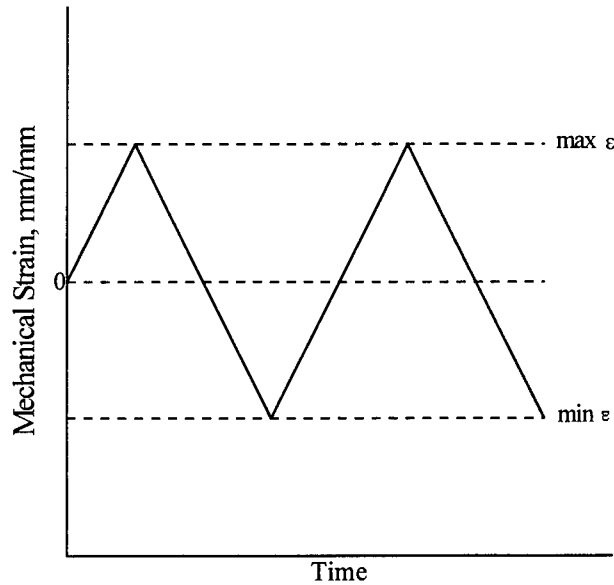


**Figure 1. Tension-Compression Wave Form**

The approach taken in this study was to perform fatigue tests at several different strain ranges, on three different  $V_f$ 's of 0.15, 0.25, 0.42. Comparisons were made between fatigue life and damage mechanisms for these three  $V_f$ 's. Fatigue lives were compared with normalized S-N curves for each  $V_f$ . Fractography and microscopy were used to determine damage mechanisms for the different strain ranges, and then compared for each  $V_f$ .

This document is arranged in the following manner. Chapter two provides a background of TMC research that details where this study contributes to the overall evaluation of the SCS-6/Ti-15-3 composite system. Chapter three discusses preparation of the test specimens from the laminate plate and the facilities used to perform the tests. Also in chapter three is a description of the tests performed and the collection of experimental data. Chapter four is divided into sections detailing the macroscopic and



microscopic evaluation of the specimens. Comparison to data from other studies is also given in this chapter. Chapter five draws conclusions from observations and analysis performed in this study. A summarization of the study and recommendations for follow-up research conclude the chapter. Other important additional information is given in the Appendix following Chapter five.

## 2. Background

This chapter provides a background summary of studies conducted on the SCS-6/Ti-15-3 composite system. Studies reviewed are limited to ones with direct impact upon the present study, and are therefore those with an emphasis on fatigue life and damage mechanisms. Two sections are presented; one for tension-tension fatigue and one for tension-compression fatigue.

### 2.1 Tension-Tension Fatigue

#### 2.1.1 Load Control Mode

Pollock and Johnson characterized the tension-tension fatigue behavior of three layups of SCS-6/Ti-15-3 composite at 650°C [28]. Laminate lay-ups of  $[0]_8$ ,  $[0/90]_{2S}$ ,  $[0_2/\pm 45]_S$  and  $[0/\pm 45/90]_S$  were tested under load control with stress ratio,  $R = 0.10$ . They concluded that the  $0^\circ$  degree fiber bundle stress controlled the composite fatigue life. The fiber bundle stress data from all lay-ups collapses into a single scatter band when plotted as a function of cycles to failure. High strain/short life specimens exhibited multiple fiber failures with no matrix fatigue cracking. Low strain/long life specimens exhibited no fiber failure away from the fracture surface and extensive matrix fatigue cracking.

Gayda and Gabb investigated the zero-tension fatigue behavior of unidirectional SCS-6/Ti-15-3 at room temperature and 550°C for  $V_f$ 's of 15%, 37%, and 41% [13]. They found that higher fiber content increased fatigue life on a stress basis at both temperatures. At 550°C, all fatigue data collapsed into one curve on a strain basis while

minor differences were found at room temperature. These differences were related to residual stress levels, fiber spacing, and fiber bridging [13].

Castelli and Gayda investigated fatigue behavior of unidirectional SCS-6/Ti-15-3 with a  $V_f$  of 35% at 427°C. A few specimens were pure matrix on the outside, with fibers only in the central core that yielded an effective fiber volume of 20% [5]. These clad specimens were fabricated by consolidating the material into a plate with alternating strips of pure matrix and composite. The specimens were machined by cutting through the matrix portions that contained no fibers so there were no exposed fibers or cut fiber ends on the exterior of the specimen. Essentially the specimens had a pure matrix casing. The fatigue lives of the clad and unclad specimens were equivalent at higher strain ranges, but the clad specimens had shorter lives at lower strain ranges. This was possibly due to accelerated crack propagation in the composite core from a matrix crack that initiated in the cladding. For all specimens, crack propagation was the primary failure mechanism [5].

Majumdar and Newaz performed tension-tension tests on  $[0]_8$  laminate with 15%, 35%, and 41%  $V_f$  at room temperature and 538°C [24]. These data were obtained in a vacuum, which is likely to increase fatigue life due to lack of oxidation of the fiber/matrix interface. Their data showed that SCS-6/Ti-15-3 fatigue life can be divided into three regimes, as done for other material systems [1,31]. Regime 1 is a short life region where fracture is dominated by statistical fiber overload and failure. Regime 2 ranges from approximately 2,000 to 500,000 cycles for tension-tension fatigue where fiber-bridged matrix fatigue cracking is the dominant damage mechanism. Fatigue lives of greater than

1,000,000 cycles fall into Regime 3, where crack initiation and propagation are not severe enough to cause failure of the specimen. This is also referred to as run-out, where tests are stopped before failure. This general fatigue response diagram is shown in Figure 2 [24]. The shaded area represents the data scatter associated with fatigue testing.

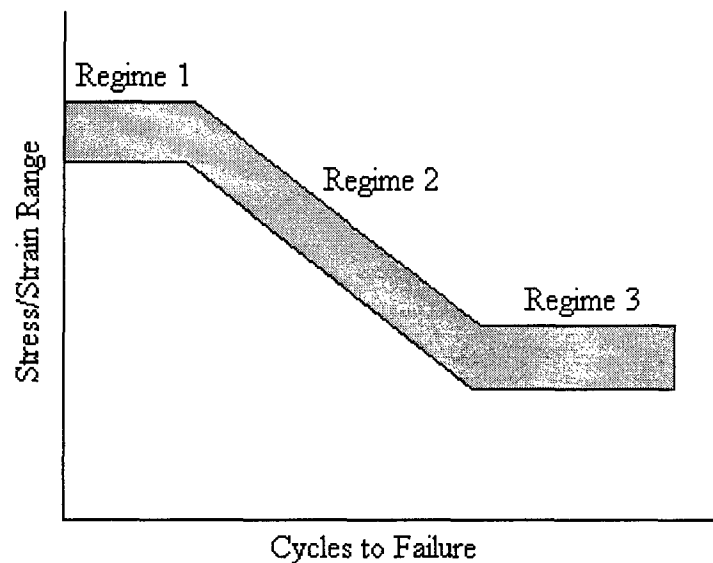


**Figure 2. Three Regimes of Fatigue for SCS-6/Ti-15-3**

Majumdar and Newaz had other important findings [24]. Perhaps most revealing was the observation that fatigue life is controlled by the strain range imposed on the specimen from the applied loading, rather than the stress range due to the applied load. This conclusion is supported by the collapse of the three fiber volume fractions' data into a single scatter band when plotted on an imposed strain range basis [24]. They also showed that, at high temperature, composite life is significantly shorter than matrix life for all strain ranges. Initially, this would suggest that any addition of reinforcing fibers is

detrimental to fatigue life. However, the matrix in the TMC was undergoing fully-reversed stresses [24], while the pure matrix tests had a strain ratio of  $R_\epsilon = 0$ . So this was an improper basis of comparison.

In addition, strain ratchetting was found to be a characteristic feature of the high temperature tests. Strain ratchetting occurs because of time-dependent relaxation of the matrix, causing the fibers to carry more of the load and deformation, which leads to an increase in mean strain [24]. This strain ratchetting dominates the fatigue life in Region I of the S-N diagram. The residual stresses in the TMC after consolidation are tensile in the matrix and compressive in the fiber because of different thermal expansion coefficients. In the first cycle in Region I, the matrix plastically deforms, so that upon unloading, the matrix goes into a compressive stress state. This leads to a tensile stress in the fibers, bringing them closer to their failure strain. Repeated cycling leads to strain ratchetting and fiber breakage without matrix cracking.

Important damage mechanisms at elevated temperature were found to be reaction zone cracks in the fiber/matrix interfacial zone, where slip bands initiated; cracks in the brittle Mo-weave; and fiber cracking in the high strain ranges.

### **2.1.2 Strain Control Mode**

Sanders evaluated the fatigue response of the unidirectional SCS-6/Ti-15-3 composite at 427°C under a zero-tension, strain-control mode [30]. Zero-tension control was achieved by increasing the minimum strain throughout the tests so that the thin

specimens never experienced a compressive load. Therefore, each specimen was subjected to a decreasing strain range over the course of a test.

Sanders found that matrix plasticity occurred when the strain level was greater than 0.55% [30]. Fiber-matrix interfacial damage was found to be a dominant damage mechanism and was a function of the maximum applied strain. This interfacial damage was in the form of debonded fibers. Oxidation caused embrittlement of the interface, so when a transverse crack reached the fiber, it grew longitudinally along the fiber and debonded it from the surrounding matrix. Sanders defined the failure mechanisms and assigned them to different portions of the  $\epsilon$ -N diagram, just as Majumdar and Newaz did [24].

## **2.2 Tension-Compression Fatigue**

### **2.2.1 Load Control Mode**

Kraabel studied the fatigue behavior of unidirectional, 35%  $V_f$  SCS-6/Ti-15-3 composite under fully-reversed, load-controlled conditions [17]. Fatigue lives of the tension-compression (T-C) specimens were found to be shorter than the tension-tension tests at the same maximum stress level for both room temperature and 427°C. The fracture surfaces for these T-C specimens exhibited portions of matrix fatigue cracking and fiber pullout with tensile matrix rupture. The ratio of these damage mechanisms depended on the applied stress, with the lower stress specimens dominated by matrix cracking.

Like Sanders [30], Kraabel constructed a fatigue life diagram which was divided into three sections as shown in Figure 3. Region I is dominated by fiber fracture. Region II was subdivided into two sections, IIa and IIb. Region IIa is dominated by short matrix cracks and Region IIb specimens exhibited long matrix cracks. Long matrix cracks span through the thickness of the composite and several columns of fibers. Short matrix cracks are arrested before bridging more than a few fibers. Region III falls below the matrix fatigue limit where fatigue lives are greater than 1,000,000 cycles, or cycle run-out.

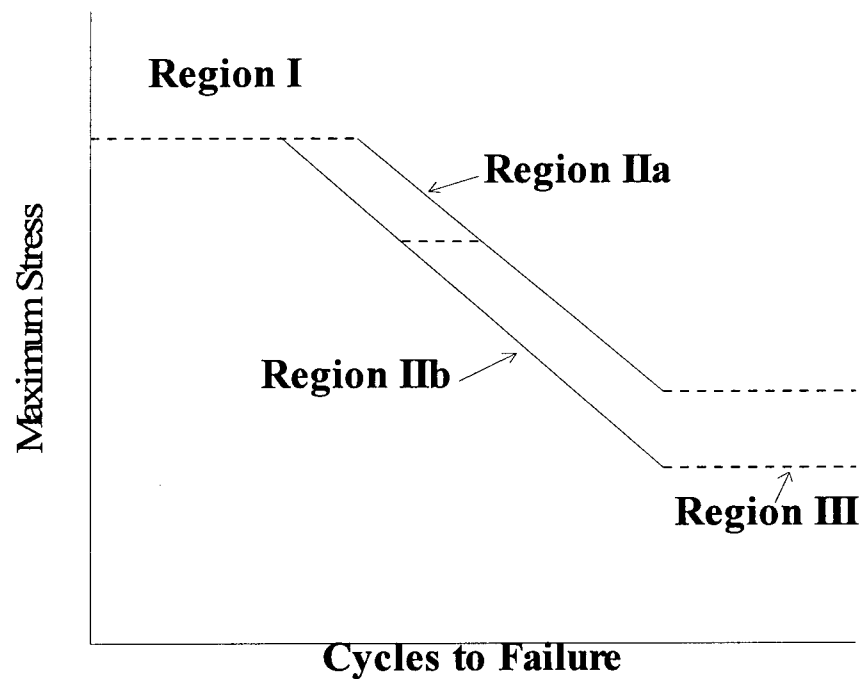


**Figure 3. [0]<sub>s</sub> Tension-Compression Fatigue Life Curve at 427°C**

### 2.1.2 Strain Control Mode

Lerch and Halford studied  $[0]_{32}$ , SCS-6/Ti-15-3 laminate at 427°C under fully-reversed, strain- and load-controlled conditions [18]. The thickness of these specimens prevented buckling under compressive loads. No difference was found between the load and strain control modes for this 35%  $V_f$  composite. Matrix cracking, typical of subcritical crack growth, was found to be the operative damage mechanism for the fully-reversed tests. Subcritical crack growth, or fatigue cracking, occurs with load cycling on the specimen that is below the failure load. This fatigue is characterized by a steadily increasing crack growth rate from initiation until the critical crack length is reached, and the remaining uncracked material fails in tensile overload.

For comparison, the fatigue life was plotted based on strain range, resulting in tension-compression lives that are approximately five times longer than strain control, zero-tension lives, and ten times longer than stress control, zero-tension lives. The strain range for the load-controlled tests was taken from the strain data obtained at 50% of life. Because the load-controlled specimens' had a stabilized strain range throughout the final 80% of life, a strain range comparison using the 50% life stabilized values was considered a valid comparison. Also, the addition of fibers to the matrix had only a slight adverse effect on the isothermal tension-compression fatigue life. This difference is a result of more damage initiation sites from the processing of fibers into the matrix. With the laminate having similar fatigue life to the matrix, it suggests the ability of the matrix to resist cyclic loading governs composite life under the failure strain of the fibers, approximately 0.9% [18].



Jackson performed several tests on the SCS-6/Ti-15-3 composite system under fully reversed, strain control condition at 427°C [14]. These tests of the  $[0]_8$ , 35% fiber volume fraction laminate agreed with the results of Lerch and Halford discussed in the previous paragraph. Jackson found fiber dominated failure at strains above 0.50%, with fracture surfaces exhibiting matrix necking and extensive fiber pullout. Below strains of 0.50%, matrix cracking was dominant and increased in density with decreasing applied strain. When compared to load control data at similar stress ratios from other research, it was shown that the damage mechanisms were independent of control mode [14]. Jackson also found that fatigue life of the composite is independent of control mode for tension-compression loading.

To date, there has not been any published investigation of the effect of fiber volume fraction on fatigue of the unidirectional SCS-6/Ti-15-3 composite under fully-reversed strain-control mode. An understanding of how the variation of constituents in the composite affects fatigue life and damage mechanisms must be developed. It was primarily with these goals in mind that the current study was undertaken.

### 3. Experiments

The purpose of this chapter is to give a detailed description of the material, test equipment, and procedures that were used in this study. The MMC specimen's composition, preparation and geometry are described. The test equipment, including the AFIT buckling guide, is also discussed. Finally, the experimental procedures that are required to perform tension-compression testing and the post-test specimen preparation are described.

#### 3.1 Material Description

Three different fiber volume ratios of an 8-ply unidirectional,  $[0]_8$ , layup were investigated in this study. A schematic of the unidirectional layup is shown in Figure 4, where all of the reinforcing fibers are parallel to the loading axis. The MMC is composed of silicon carbide fibers, SCS-6, in a titanium metal matrix, Ti-15-3. The fibers have a nominal diameter of 140  $\mu\text{m}$  and are built up from an inner core encapsulated in bulk SiC with alternating layers of silicon and carbon coatings. Due to reactivity between the titanium alloy and the silicon carbide fiber during processing, a protective coating on the fiber must be used. This coating interface is relatively weak and has a large role in the fatigue properties of the composite. The exact composition of the matrix material is: Ti-15V-3Cr-3Al-3Sn, weight percentage. This is a metastable beta Ti-alloy that contains a very fine omega phase. Alpha phase particles are known to precipitate in the microstructure at temperatures above 300°C, but do not have a

significant effect on the fatigue life of the MMC at room temperature [24]. Table 1 lists the mechanical properties of the fiber and matrix.

**Table 1. Fiber and Matrix Properties**

	SCS-6 FIBER	Ti-15-3 MATRIX (RT)	Ti-15-3 MATRIX (427°C)
<b>MODULUS (GPa)</b>	395	90	80
<b><math>\alpha</math> (<math>10^{-6}</math> mm/mm/<math>^{\circ}</math>C)</b>	4.86	10	10
<b><math>\nu</math></b>	0.25	0.36	0.36
<b><math>\sigma_{ys}</math> (MPa)</b>	--	800	525

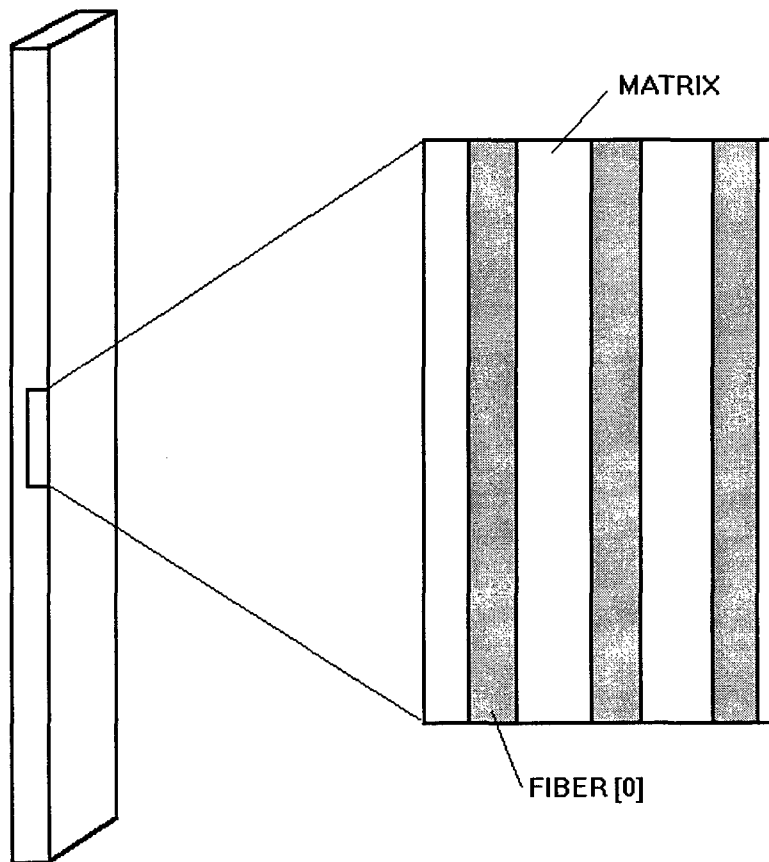


**Figure 4. Schematic of Unidirectional [0°] Specimen Orientation.**

The three nominal fiber volume ratios studied are 15%, 25%, and 42%. The  $V_f$  can be controlled by consolidating the MMC plates with different spacing between the individual fibers or varying the matrix foil thickness. The three MMC plates evaluated in this study were manufactured by Textron Specialty Materials Incorporated using a proprietary Hot Isostatic Pressing (HIP) method. Each plate is made by arranging the silicon fiber tape in alignment between layers of Ti-15-3 foil matrix and heating under pressure and vacuum to consolidate. This process is known as the foil-fiber-foil method. The unidirectional SCS-6 fiber tape is aligned by a cross-weave material. This cross-weave is absorbed into the laminate during consolidation. The cross weave in this study was Molybdenum (Mo) in the 15% and 42% MMC's, and Ti-Niobium for the 25% MMC. Non-destructive X-ray evaluation of the MMC plates revealed that the molybdenum cross-weave in the 42% plate was damaged during consolidation in the HIP. Cracking around the fibers and voids in the matrix near the Mo-weave were present. It is assumed that this damage is so minor as to have no effect on the fatigue life characteristics of the material. This presumption will be verified after examination of the test results.

### **3.2 Specimen Design and Preparation**

A dogbone specimen geometry with a reduced gage cross-sectional area was chosen for all tests performed in this study. Previous studies have shown that a dogbone geometry facilitates specimen failure in the gage section for tension-compression testing [24]. A driving force in the specimen design is to minimize stress raisers on the specimen

edge while reducing the gage area to control specimen failure location. The way this is achieved is to hold the shoulder radius as large as possible. Several studies have shown the dogbone design to be effective in fatigue characterization testing [14,24]. Figure 5 shows the dogbone specimen design utilized in this study.

The specimens were first cut from large MMC plates into a nominal rectangular coupon size using Electro-Discharge Machining (EDM) techniques. Next, the dogbone cut was made into the sides of the specimens also using EDM. Then the final 0.127 mm was ground off with a diamond router tool to finish the specimen edge and remove any burn zone from the EDM. Nominal geometry dimensions of 152.4 mm long in the 0° direction and 12.7 mm wide in the grip sections were specified.

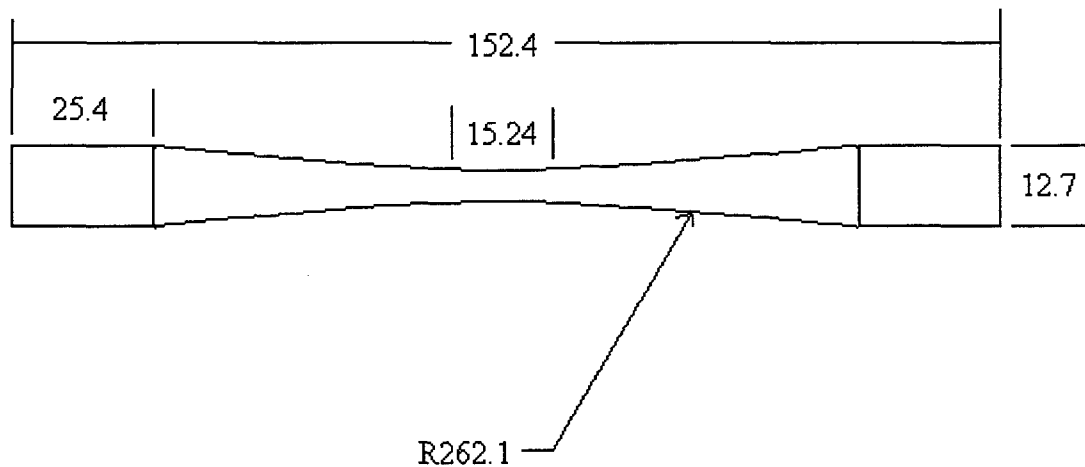


**Figure 5. Dogbone Specimen Geometry for This Study (Dimensions in mm)**

Several studies have shown an increase in modulus of the material during elevated temperature fatigue testing [8,14]. An effort was made to minimize this change in

behavior by heat treating these specimens. The heat treatment used in this study consisted of wrapping the specimens individually in tantalum foil and holding at 700° C in an inert Argon gas atmosphere for 24 hours. Lerch and Saltsman have shown that the microstructure of the material is stabilized without changing the mechanical response of the material with this heat treatment [19]. However, the stabilized microstructure cannot prevent the precipitation of the alpha phase particles which alter the modulus of the composite [24]. So the heat treatment stabilizes the microstructure at the machined areas in the specimen, while the modulus changes that are a result of alpha phase precipitation do not significantly influence fatigue life.

After heat treatment, the MMC specimens are ready for test preparation. The final step in the process is to fine grind the edges to remove any protruding fibers and to smooth out any indentations that would cause a stress concentration in the specimen edge. This is done with the use of a low speed Struers Transpol-2 hand polisher with 45 µm silicon carbide sandpaper discs and water lubricant. Any further polishing was deemed unnecessary, and in fact, would make it difficult to get a positive, non-slipping contact for the extensometer.

### **3.3 Buckling Guide Description**

The AFIT buckling guide was originally designed by Boyum [2]. This was designed to provide out-of-plane support of a slender specimen while not interfering with the axial test load and strain on the specimen. Modified versions of the buckling guide

were used successfully by Dennis, Kraabel, and Jackson [8,14,17]. Their designs were optimized to reduce thermal mass for possible thermomechanical fatigue.

The 152.4 mm length  $[0]_8$  specimens used in this study are too long to be unsupported in fully-reversed compression. Since a larger buckling guide was needed to support the longer specimens, one was designed from scratch with emphasis on rigidity and durability. Figure 6 shows the buckling guide used in this study. It was made of two 4130 steel sections, upper and lower. These sections clamp independently to the specimen with machine screws and interface with a sliding fork mechanism. As the specimen elongates, the buckling guide allows unhindered axial movement through the fork. This gives a true stress-strain history with out-of-plane support.

### **3.4 Test Setup**

All elevated temperature tests were performed on a MTS 808 electro-mechanical screw-driven test machine equipped with a 100 kN load cell. Water-cooled hydraulic friction grips were used to hold the specimen. A MTS 632.53E ceramic-rod elevated temperature contact extensometer was used to obtain strain data. This extensometer had a gage length of 12.7 mm, with upper and lower strain limits of 0.010 mm/mm. A contact force of 260 grams is applied by the extensometer through a supporting leaf spring. Test temperature was maintained with water-cooled quartz lamps under Barber-Colman 560 controllers with K type thermocouples. The test software was a program developed in-house using National Instruments' Labview for Windows 3.11. A Zenith 486 computer

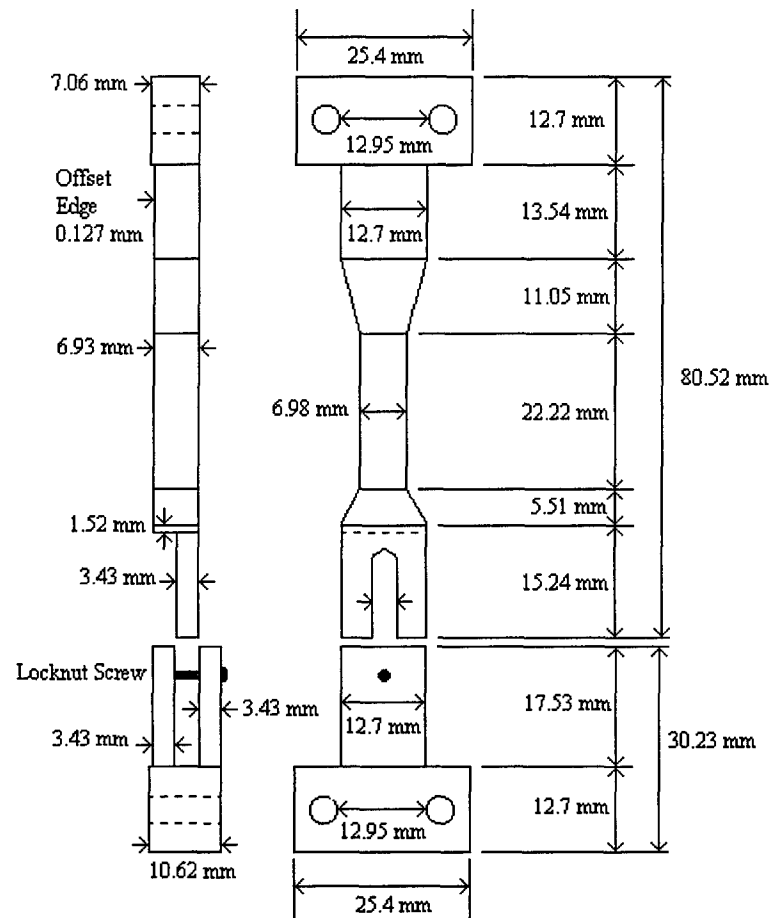


**Figure 6. AFIT Buckling Guide used for this study**

runs the software and stores the data acquired. The user specifies all aspects of the test including R-ratio, temperature, strain level, data acquisition interval, etc.. The test apparatus is shown in Figure 7.

Data acquisition is performed by the computer at user-defined intervals. The individual data cycles are written to the computer disk with the cycle count as the



filename. The software also creates a minimum/maximum file that includes stress, strain, and temperature at each data interval.

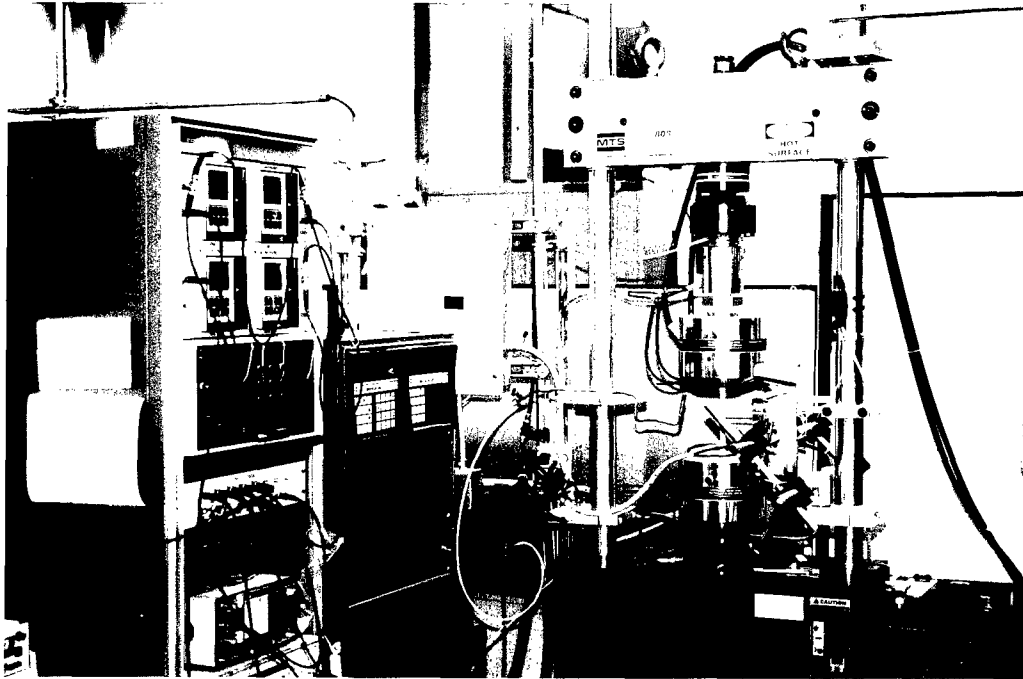


**Figure 7. Test Apparatus**

Two thermocouples were spot welded to the specimen buckling guide for test temperature feedback. Once the specimen was loaded into the test stand with the thermocouples and buckling guide in place, the 12.7 mm gage length ceramic arm extensometer was placed on the specimen edge and zeroed. A test temperature of  $427 \pm 2^\circ\text{C}$  was maintained for the test duration. A soak-time of 30 minutes was used prior to each test to allow any temperature gradients to stabilize and ensure even heating in the gage section. The temperature distribution was monitored with three thermocouples: one

at the center of the gage section, one on the lower face of the specimen at the end of the gage length, and one on the opposite face and gage end of the specimen. This ensured that the gage length was at the desired 427°C. There was no concern with the temperature distribution outside this gage length because of the dogbone geometry. A higher temperature and smaller cross-sectional area facilitates failure in the gage length. The initial cycle for each test was performed manually to obtain an initial modulus. Then the program parameters were entered, and the software began ramping to the starting strain to begin the test.

### **3.5 Tests**

The tests in this study were performed under fully-reversed ( $R = -1.0$ ) strain control with a strain rate of 0.001 mm/mm/s. Four strain levels were tested for the three different fiber volume fractions of MMC. A triangular waveform was used for the fatigue cycle. Table 2 shows the test matrix for this study.

**Table 2. Test Matrix**

Specimen #	Fiber Volume	Control Mode	Strain Range (%)
1B	0.15	STRAIN	0.80%
1C	0.15	STRAIN	0.60%
1G	0.15	STRAIN	0.60%
1F	0.15	STRAIN	0.70%
1H	0.15	STRAIN	1.10%
2C	0.25	STRAIN	0.60%
2D	0.25	STRAIN	0.70%
2B	0.25	STRAIN	0.80%
4B	0.42	STRAIN	0.60%
4C	0.42	STRAIN	0.70%
4A	0.42	STRAIN	0.80%
NM0102A	NEAT MATRIX	STRAIN	0.60%

### **3.6 Post Failure Analysis**

Post failure analysis consisted of sectioning the specimens and evaluating the fracture surface and polished face surface with both optical and Scanning Electron Microscopes (SEM). The location of these sections is shown in Figure 8.

The sections were cut using a high speed Buehler saw with a diamond impregnated saw blade. The fracture surface was then cleaned in an ultrasonic cleaner to remove any contaminants. This was then mounted on a SEM observation platen with conductive silver paint. The fracture section was then ready for examination.

The face sections were mounted in Buehler Konductomet II, a conductive mounting powder. A Buehler mounting press cured the section in the mounting powder under high pressure and temperature. This resulted in a very hard mount supporting the section for grinding and polishing. The first grinding stage used a 45 $\mu$ m diamond slurry on a metal mesh screen to expose the first fiber layer. Subsequent polishing stages used 9, 3, and 1 $\mu$ m diamond slurries respectively on an automatic polishing wheel to remove

any remaining scratches. Final polishing was conducted on a Buehler Vibromet with Buehler Mastermet finish polishing compound. The specimens were then ready for examination in the optical light microscope.

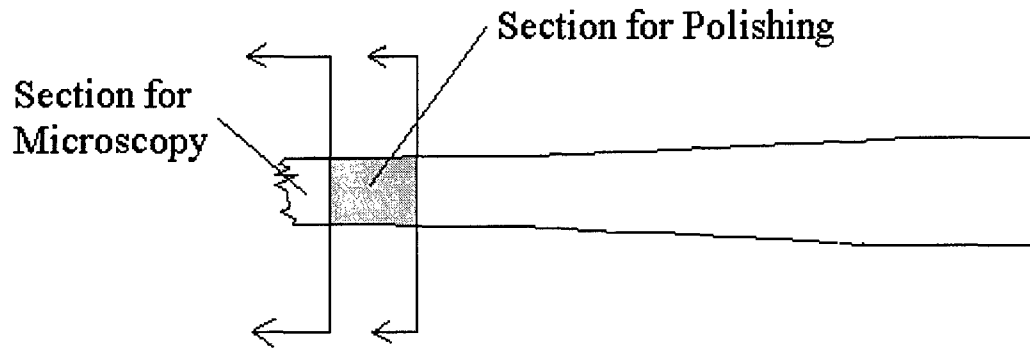


**Figure 8. Location of Sections for Specimen Analysis**

## 4. Results and Discussion

The results from macro-mechanical and microscopic analysis will be presented for the  $[0]_8$ , SCS-6/Ti-15-3 specimens tested in this study. The macro-mechanical section will include modulus, stress, and strain histories during fatigue cycling. The microscopic discussion will include details of the damage mechanisms and causes of specimen failure. The macro-mechanical response and microscopic evaluation will be compared among the three different fiber volume fractions.

### 4.1 Macro-mechanical Analysis

The modulus of a material is a measure of how stiff it is. For a given applied stress the material will strain a commensurate amount, related by the modulus, or slope, of the stress-strain curve. Secant modulus is a linear fit between the two endpoints of the stress strain cycle. Figure 9 shows a typical stress-strain diagram for a damaged TMC specimen. The tensile modulus is calculated from the positive linear portion of the curve-slope, while the compressive modulus is calculated from the negative linear portion of the curve-slope. For tension-compression tests with a similar compressive modulus, secant modulus is an appropriate tool used to quantify damage in the specimen. Any change in the tensile modulus will be reflected to a lesser degree in the secant modulus. Therefore, to reduce the number of parameters that tests will be compared by, all comparisons will be made on a basis of secant modulus.

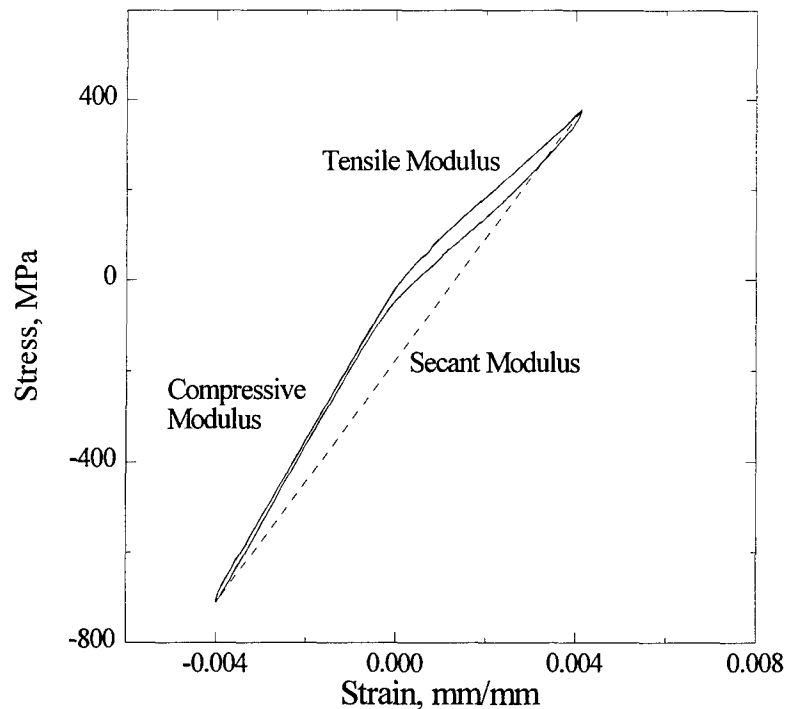


**Figure 9. Definition of Different Moduli from a Stress-Strain Curve**

#### **4.1.1 Consolidated Neat Matrix**

One fatigue test was performed on a neat matrix specimen consolidated with the same fiber-foil-fiber method used for the composite. This specimen provided the opportunity to analyze the strain-controlled, fully-reversed fatigue behavior of the matrix. The specimen was cycled at a strain range of 0.006 mm/mm. The secant modulus results are shown in Figure 10. It reveals an increase in the stiffness of the material of approximately 15.2% over the initial value. Analysis of both the tensile and compressive moduli also individually indicate the same effect. This increase is due to strain hardening or a phase precipitation in the material. It has been shown previously that an alpha phase precipitation will occur along grain boundaries in the Ti-15-3 material, making the matrix

stiffer, but more brittle [25]. No information was found in the literature on the effect of strain hardening on the modulus of the Ti-15-3 material. This matrix test result lends insight into the stiffness behavior of the composite laminate discussed later in this chapter.

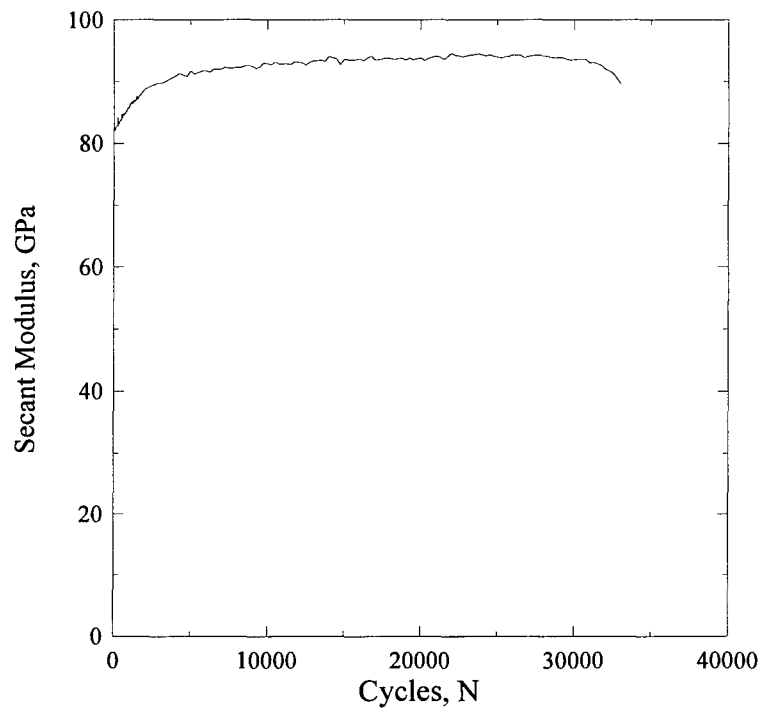


**Figure 10. Secant Modulus History of Neat Matrix**

#### **4.1.2 15% Fiber Volume Fraction**

Five fully reversed, strain control fatigue tests were performed for this portion of the study. The maximum strain, strain range, initial modulus, and cycles to failure for the five tests are given in Table 3.

**Table 3. 15%  $V_f$  TMC Test Matrix**

<b>Maximum Strain (%)</b>	<b>Strain Range (%)</b>	<b>Initial Modulus (GPa)</b>	<b>Cycles to Failure</b>
<b>0.55</b>	<b>1.1</b>	<b>123.7</b>	<b>4340</b>
<b>0.4</b>	<b>0.8</b>	<b>143</b>	<b>9121</b>
<b>0.35</b>	<b>0.7</b>	<b>162</b>	<b>21945</b>
<b>0.3</b>	<b>0.6</b>	<b>144</b>	<b>26115</b>
<b>0.3</b>	<b>0.6</b>	<b>136.3</b>	<b>40285</b>
<b>0.25</b>	<b>0.5</b>	<b>125.1</b>	<b>45189</b>

The compressive ( $E_c$ ) and tensile ( $E_t$ ) moduli histories for the test conducted at a maximum strain of 0.25% are shown in Figure 11. This figure shows that the compressive modulus increases slightly throughout the test after an initial rapid increase. Similar behavior was reported by Dennis in tension-compression testing of a cross-ply SCS-6/Ti-15-3 MMC [8], and by Jackson in tension-compression testing of a unidirectional SCS-6/Ti-15-3 MMC [14]. This compressive modulus behavior is most likely caused by closure of fatigue cracks and a lack of any other significant damage mechanisms in compression, which leaves only the hardening of the matrix to produce the slight increase over the life of the test.

Using the rule of mixtures analysis for continuous fiber, unidirectional composite lamina, the longitudinal modulus lies between the fiber and matrix moduli, and given by the equation [25]:

$$E_L = E_f V_f + E_m (1 - V_f)$$



By using the 15.2% modulus increase in the matrix due to phase transformation as seen in the neat matrix specimen in the above equation, the 15%  $V_f$  laminate is expected to stiffen 12.9% during the test. The experimental data shown in Figure 11 indicates an increase of 12.5%, very close to this value, thus this observed increase in modulus is most likely due to the phase transformation of the matrix.

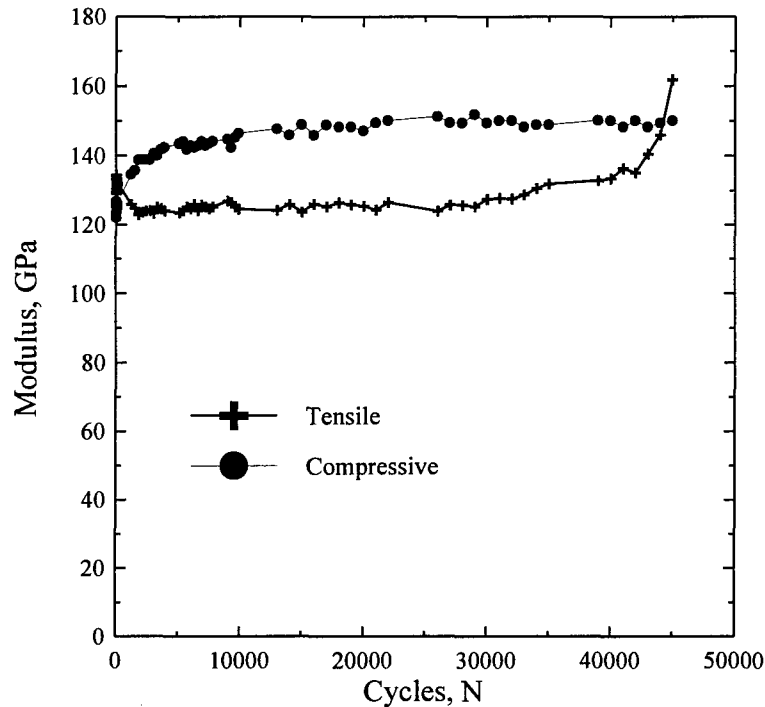


**Figure 11.  $\epsilon_{\max}=0.25\%$ ; Tensile and Compressive Modulus History**

An indication to the extent of damage in a specimen is revealed by a reduction in the modulus. Generally, matrix cracking and/or fiber breakage and pull-out will degrade the modulus. Nicholas and Ahmad have shown that a limited amount of fiber breakage will not significantly degrade the modulus unless the fiber crack opening displacement is on the order of two-to-three fiber diameters [27]. This opening displacement is measured

between the ends of the broken fiber. Later it will be shown that there was little fiber breakage and crack opening in the composite prior to failure.

Permanent strain accumulation, or strain ratchetting, is an indication of large scale fiber pull-out. Since the fibers behave linear-elastically in the strain and temperature regions for this study, a permanent strain accumulation is only possible if fiber pull-out occurs and the matrix is unable to carry the load. As a result the matrix undergoes viscoplastic deformation and the strain at zero stress has changed. It will be shown in the stress-strain loop figures later in this section that there is only minor strain ratchetting for any given test.

A lack of strain ratchetting eliminates fiber pull-out as the major cause of modulus reduction seen in some of the specimens. Therefore, this observed modulus reduction is a result of matrix cracking and/or viscoplastic deformation of the matrix.

The secant modulus history for all six tension-compression tests is shown in Figure 12. The average initial secant modulus for the 15% fiber volume fraction material is 130.5 GPa. The 15%  $V_f$  secant modulus plot shows steady or slightly increasing values of secant modulus prior to specimen failure. The only exception is the test performed at a maximum strain of 0.4% strain.

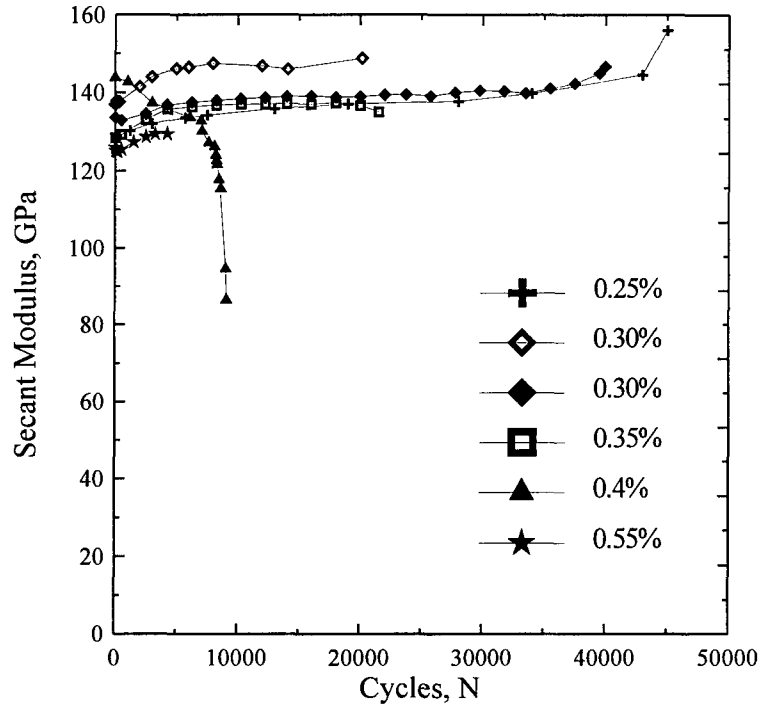


**Figure 12. Secant Modulus Histories for 15%  $V_f$  Tests**

In order to understand the mechanical modulus response of the composite in more detail, an attempt was made to separate the two competing mechanisms at work; matrix hardening and damage. The data from the specimen tested at 0.3% strain, the same strain level as the neat matrix specimen, was modified by subtracting out the percentage of modulus increase in the neat matrix specimen cycle for cycle. This result is shown in Figure 13.

This figure reveals that initially there is an overall reduction in the secant modulus due to viscoplastic matrix deformation until the modulus response reaches equilibrium at around 3,000 cycles. At this point the matrix has relaxed and transferred a portion of the load to the fibers. From that point the modulus drops only slightly over the next 30,000 cycles, which is the initiation and propagation of cracks in the matrix.

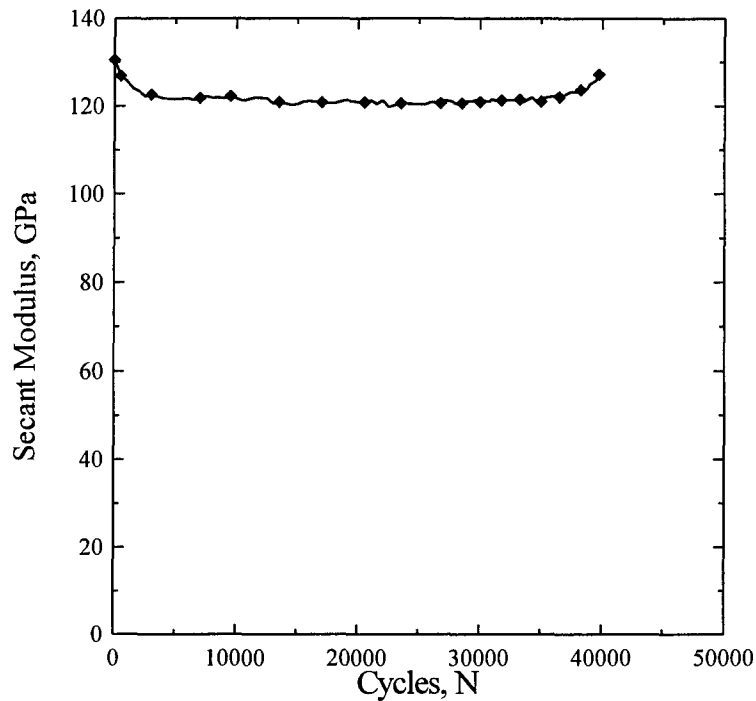


**Figure 13. Modified Secant Modulus for 0.3% Test**

The subsequent rise in modulus at the end of the test is discounted due to control problems. This issue is addressed later in this section.

There are reservations about the validity of just subtracting out the matrix hardening behavior to clarify the damage response of the material, especially because there are fiber/matrix interface effects and changes in the load carrying capacity of the matrix due to the viscoplastic deformation. However these effects are minor in comparison to the gross impact on modulus that the matrix hardening has, as well as being beyond the scope of this investigation.

This damage behavior of competing mechanisms is typical of all the tests performed with the exception of the 0.4% maximum strain test. The rapid decrease in modulus after viscoplastic deformation indicates that more matrix cracking occurred at

this strain level. Microscopy discussed in the next section will show the higher matrix crack density that results from the higher strain level.

The stress-strain response for the test conducted at a maximum strain of 0.4% is shown in Figure 14. It shows that as fatigue progresses, less stress is needed to maintain

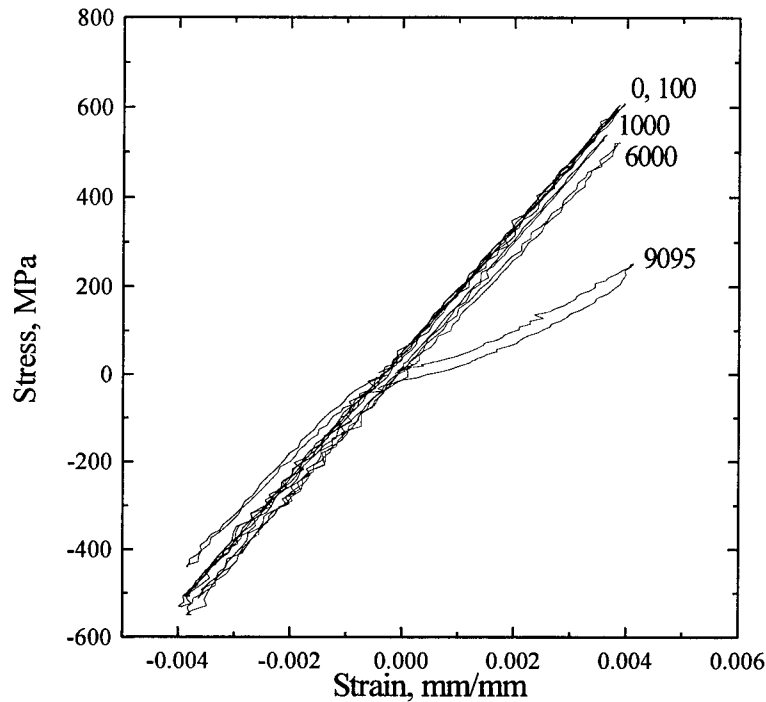


**Figure 14. Stress-strain loops for 0.4% maximum strain test**

the strain level on the specimen, while the compressive portion of the cycle remains fairly constant. This means that there is significant damage in the specimen, so much that the modulus is approaching that of the fiber bundle. Therefore the matrix is carrying little or no load before failure. It also shows increasing hysteresis with the consecutive cycles. Hysteresis is the width of the slender stress-strain loop. Wider loops mean more hysteresis, which is an indication of how much energy the specimen dissipates during a

cycle. Contributions to this dissipation are frictional rubbing between the fiber and matrix at the interface, and opening and closing of the matrix cracks, among others. The stress-strain history of this specimen concurs with the trend found in the secant modulus in Figure 12, both show a large drop in the modulus of the composite before failure.

The stress-strain response of the specimen tested at a maximum strain of 0.3% is shown in Figure 15. It shows a constant compressive modulus throughout test life,

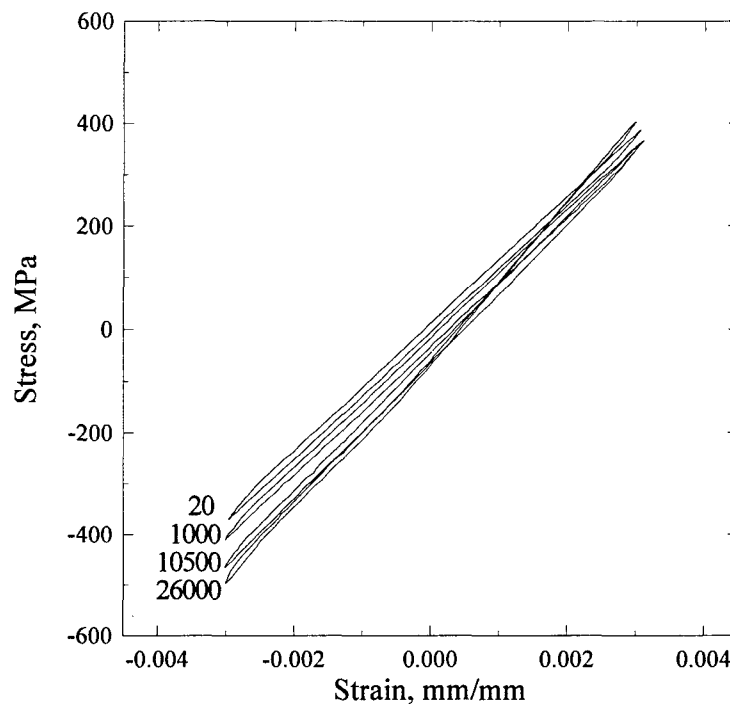


**Figure 15. Stress-strain Loops for 0.003 mm/mm test**

as well as strain ratchetting up until failure. This strain ratchetting is exhibited in the increasing compressive stress at the zero strain level as the test continues to cycle.

Interesting to note is the increasing tensile modulus over specimen life with no degradation before failure. The stress range at less than 100 cycles before failure was at

its largest value of any time during the test. This behavior cannot be attributed to the strain hardening of the matrix discussed previously because the compressive modulus would have been equally affected. The only possible explanation is the test control mode itself.

With a strain-controlled test, the test frame relies on feedback from the extensometer to apply the necessary load. Therefore, damage occurring in the gage length of the extensometer must be representative of global damage in the specimen. If a large crack or cracks develop outside of the gage length, a false reading of global specimen strain will result. The impact of this control phenomenon is discussed in more detail in the conclusions section, but from this it can be said that if the tensile modulus is stiffer than the compressive modulus, there must be a large crack outside of the gage length of the extensometer.

#### **4.1.3 25% Fiber Volume Fraction**

Three fully reversed, strain control fatigue tests were performed for this portion of the study. Table 4 lists the macromechanical data for the tests on this fiber volume fraction. The secant modulus histories for all three specimens are shown in Figure 16. The average initial secant modulus is 173.6 GPa. This figure reveals a decrease in the secant modulus with an increase in the applied maximum strain, the same trend as the 15%  $V_f$ . Therefore, there appears to be more matrix cracking in the higher strain range tests. Microscopic examination will show large and greater number of matrix cracks in the 0.4% maximum strain specimen. Also shown in Figure 16 is an increase in the secant modulus as predicted by the behavior of the hardening matrix. This increase is

approximately 8% in the 0.30% and 0.35% maximum applied strain tests. Rule of mixtures for composite analysis predicts the 8% increase.

**Table 4. 25%  $V_f$  TMC Test Matrix**

Maximum Strain (%)	Strain Range (%)	Initial Modulus (GPa)	Cycles to Failure
0.4	0.8	170.4	22049
0.35	0.7	171.0	26543
0.3	0.6	169.8	60640

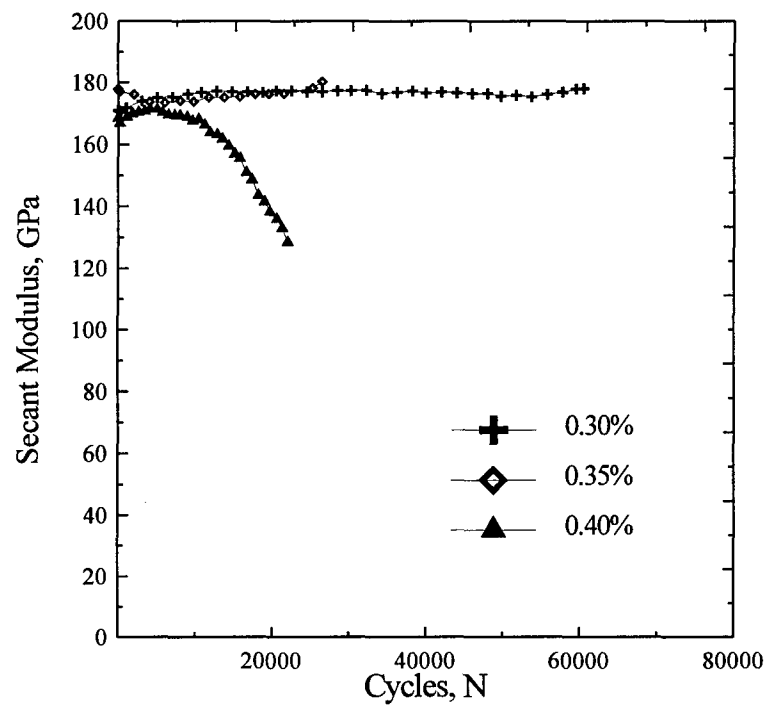


**Figure 16. Tensile Modulus Histories for 25%  $V_f$  Tests.**

Figure 17 shows the results of the attempt to isolate the competing fatigue mechanisms of matrix hardening and damage accumulation, as was done for the 15%  $V_f$ .



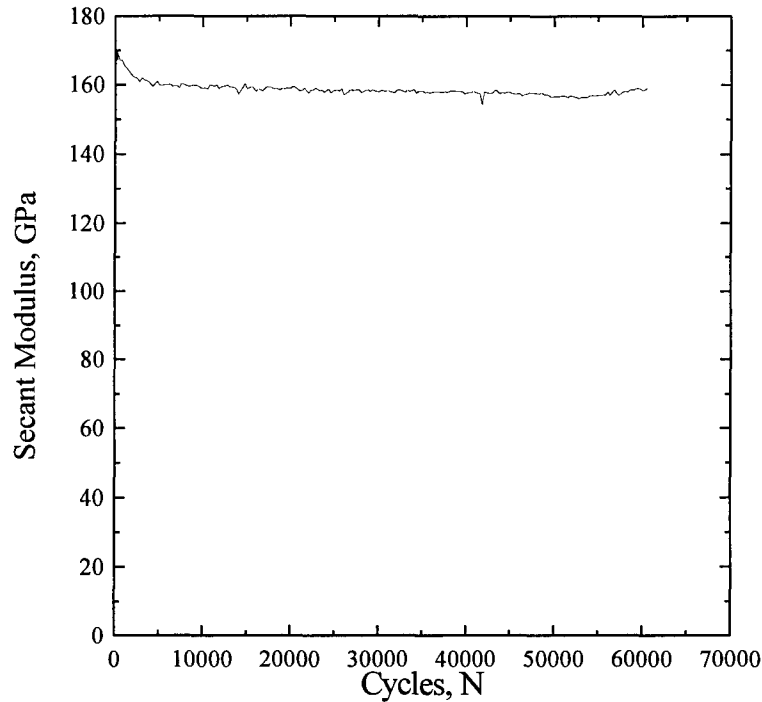


**Figure 17. Modified Secant Modulus of the 0.3% Test**

This data is from the 0.3% strain test and was modified by subtracting out the matrix hardening effect on the modulus using the neat matrix test data. The 25% fiber volume fraction was taken into account when using the rule of mixtures. Figure 17 exhibits the same damage accumulation response as the 15%  $V_f$ . There is an initial significant decrease in modulus of approximately 7% due to viscoplastic deformation of the matrix. Once this deformation has stabilized, there is a steady, slight degradation in the modulus until failure, indicating fatigue crack initiation and growth. The changes in modulus in the last 10,000 cycles of life are discounted due to the strain-control problems that arise when the material is near failure.

The stress-strain response of the 0.4% maximum applied strain test is shown in Figure 18. Regression of the maximum tensile load on the specimen as it fatigues indicates matrix damage. A damaged specimen will carry less load, and therefore a defined strain level will not require the higher load that an undamaged specimen would. The significant reduction of maximum load in this specimen is an indication of severe matrix cracking and localized fiber breakage as the modulus of the specimen dropped below the fiber bundle modulus. The fiber bundle modulus is calculated assuming that the matrix is no longer carrying any load, therefore the modulus of the specimen is the modulus of the SCS-6 fibers multiplied by the  $V_f$ . For this 25%  $V_f$  the fiber bundle modulus is 98 GPa, and the tensile modulus of the last stress-strain cycle is 93.7 GPa. This is only possible if the fiber bundle is not intact and therefore some limited fiber

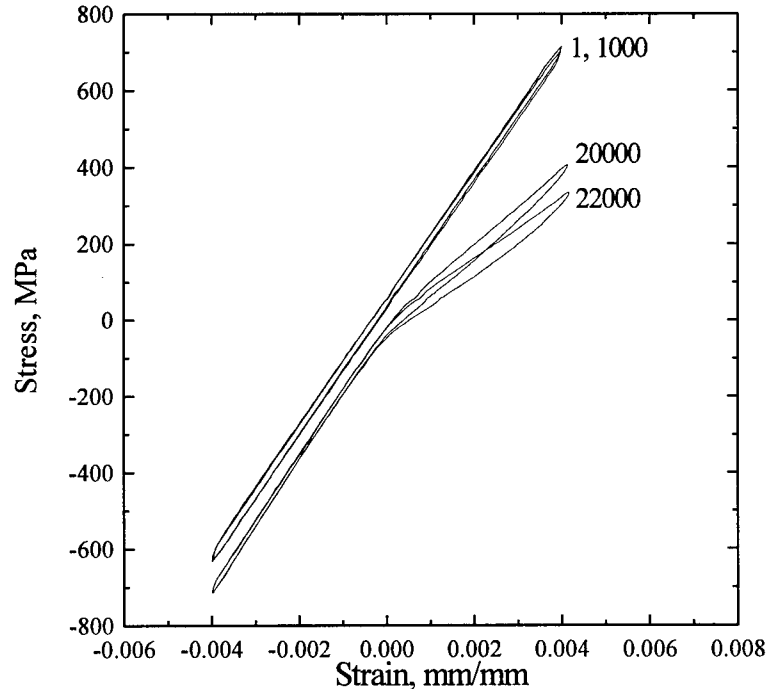


**Figure 18. Stress-strain Loops for 0.4% Maximum Strain Test**

breakage has occurred. This deduction is valid because the silicon carbide fibers behave linear-elastic in the strain ranges used in this study, and therefore the fiber modulus remains constant throughout the test. Microscopic evaluation will show the fiber cracking in the 0.4% strain specimen later in this chapter.

#### 4.1.4 42% Fiber Volume Fraction

Three fully reversed, strain control tests were performed for this portion of the study. The macromechanical data are presented in Table 5.

**Table 5. 42%  $V_f$  TMC Test Matrix**

<b>Maximum Strain (%)</b>	<b>Strain Range (%)</b>	<b>Initial Modulus (GPa)</b>	<b>Cycles to Failure</b>
<b>0.4</b>	<b>0.8</b>	<b>209.1</b>	<b>10630</b>
<b>0.35</b>	<b>0.7</b>	<b>230.0</b>	<b>26304</b>
<b>0.3</b>	<b>0.6</b>	<b>230.2</b>	<b>90069</b>

Secant modulus histories for all three specimens are shown in Figure 19. This figure reinforces the trend of decreasing tensile modulus during fatigue with increasing maximum applied strain found in the two lower fiber volume fractions. Evident in this figure is the effect of fiber volume fraction on the fatigue response of the composite. In this high 42%  $V_f$  material there is much less matrix to harden, leaving damage accumulation as the major element in modulus response to fatigue.

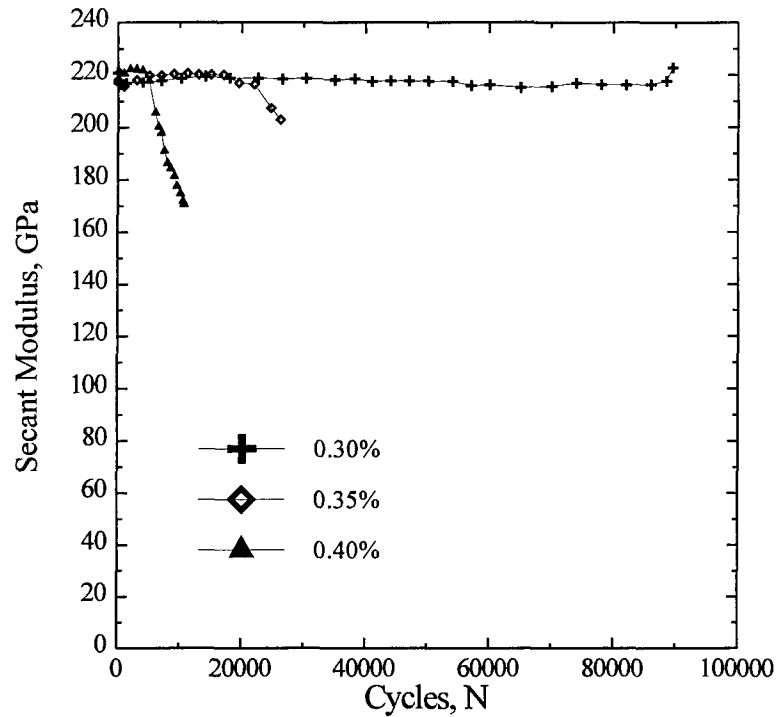


**Figure 19. Tensile Modulus Histories for the 42%  $V_f$  Tests**

The stress-strain response of the 0.40% maximum strain test is given in Figure 21.

There is a visible drop in the tensile modulus with each progressive cycle. The area enclosed by each loop, or hysteresis, is also increasing with cycles. This is another indication of damage to the composite because a wide hysteresis loop is evidence of energy dissipation in the specimen, such as crack closure and frictional heating at the damaged fiber/matrix interface.

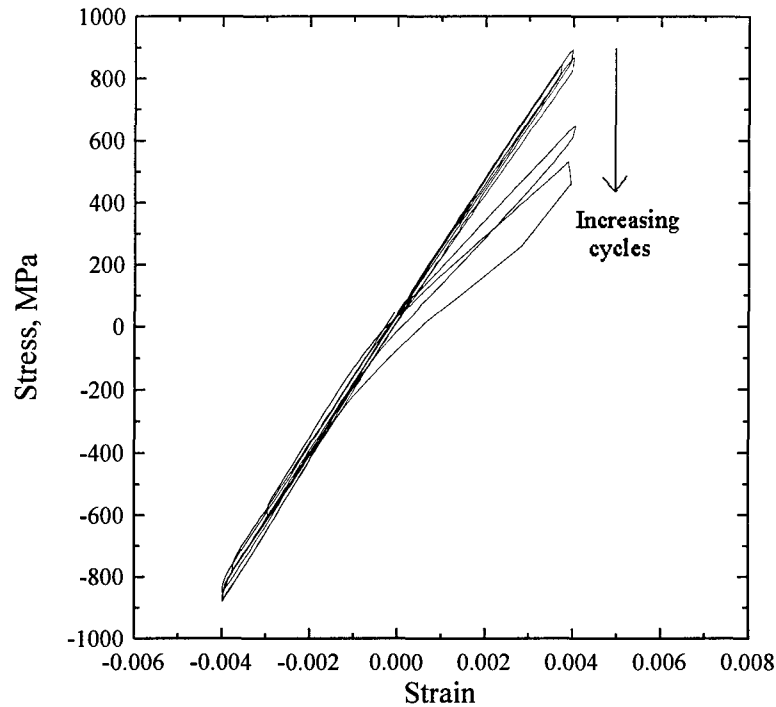


**Figure 20. Stress-strain loops for 0.40% maximum strain test**

To demonstrate the reduced affect of the matrix on the modulus response, the data from all three fiber volume fraction tests performed at a strain level of 0.3% are shown in Figure 21. Both the experimental and modified data are shown for comparison. Initially, the difference between these two moduli for the 15%  $V_f$  rapidly increases, while it is less in the 25%  $V_f$ , and much less in the 42%  $V_f$ . Also the steady state experimental and modified modulus are approximately 20 GPa apart in all cases. On a percentage basis, this shows a much greater effect in the lower fiber volume fractions.

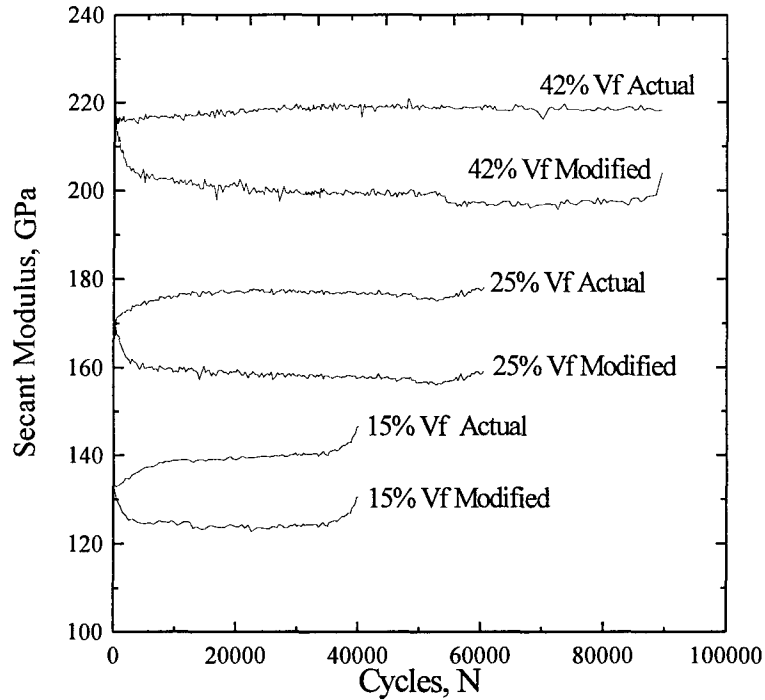


**Figure 21. Moduli for 0.3% Strain Tests for all  $V_f$ .**

#### 4.1.5 Summary

Regardless of fiber volume fraction, it is shown that tests exceeding 0.35% maximum strain were subjected to considerable damage, and modulus degradation began at approximately 50% of life. Microscopy will show that matrix cracking had a critical effect on fatigue response when the applied strain was above 0.35%. A problem with the active strain control late in fatigue life is a concern. Depending upon the crack location relative to the extensometer arms, the reduced cross-sectional area of the specimen may have been subject to a local overload as the matrix crack grew. This would accelerate damage compared to the ideal strain control test and affect the apparent modulus response. A significant change in the cycles to failure is not expected because these large

matrix cracks would become dominant only in the last fraction of fatigue life. As a result, any failure due to local overloading will not shift the fatigue life data by more than a small amount, which is within the scatter band of fatigue data.

## 4.2 Fatigue Life

An S-N diagram is a plot of the applied strain range or stress versus the number of cycles to failure for each specimen tested. Therefore, each test is represented by a single data point on the plot. The plot of strain range versus cyclic life for the 42%  $V_f$  data is shown in Figure 22 together with 36%  $V_f$  data generated in a previous study [14]. It is noted that there is little difference in fatigue life between these two  $V_f$  at any strain level. This is expected because of the minor difference in fiber volume fraction.

The S-N diagram for the tests performed on the 15%  $V_f$  specimens is shown in comparison to the 35%  $V_f$  and 42%  $V_f$  data in Figure 23. The total strain ranges vary from 0.50% to 1.10%. At higher strain ranges of 0.008 mm/mm and above, there is no significant difference in fatigue life for any  $V_f$ . However, as the strain range decreases below that level, it shows an increase in fatigue life with increases in fiber volume fraction.

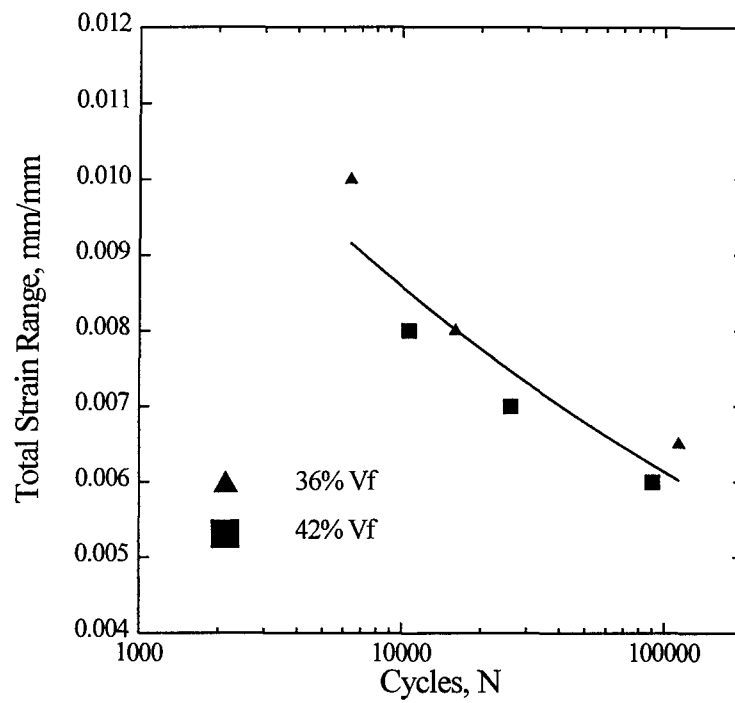


**Figure 22. S-N Diagram for 42%  $V_f$  and 36%  $V_f$**

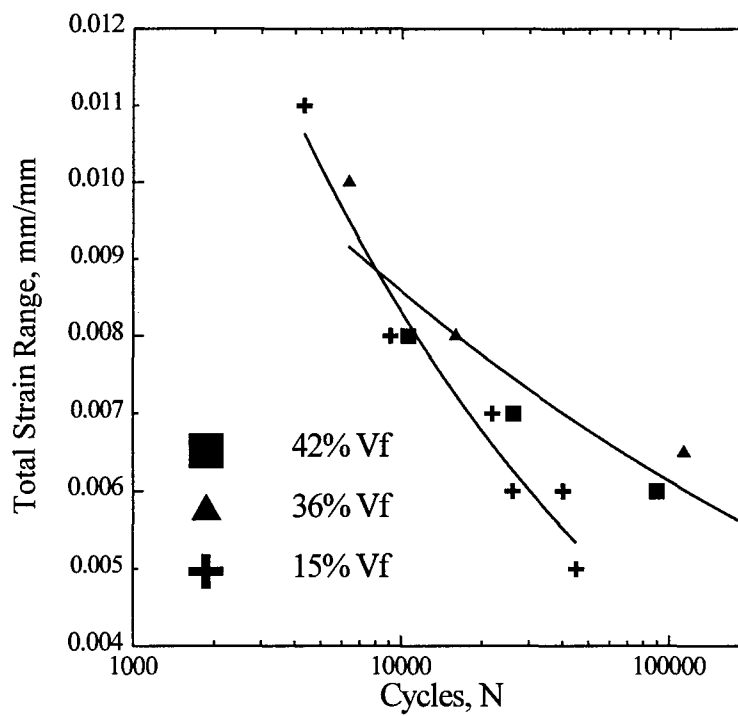


**Figure 23. S-N Diagram for 15%, 36%, and 42%  $V_f$**



The complete S-N diagram for all fiber volume fractions, including the 25%  $V_f$  specimens, is shown in Figure 24. It further reinforces the trend of increasing fatigue life with increasing fiber volume fraction at decreasing applied strain range. The 25%  $V_f$  data falls in between the 15% and 36%, 42% data, as anticipated.

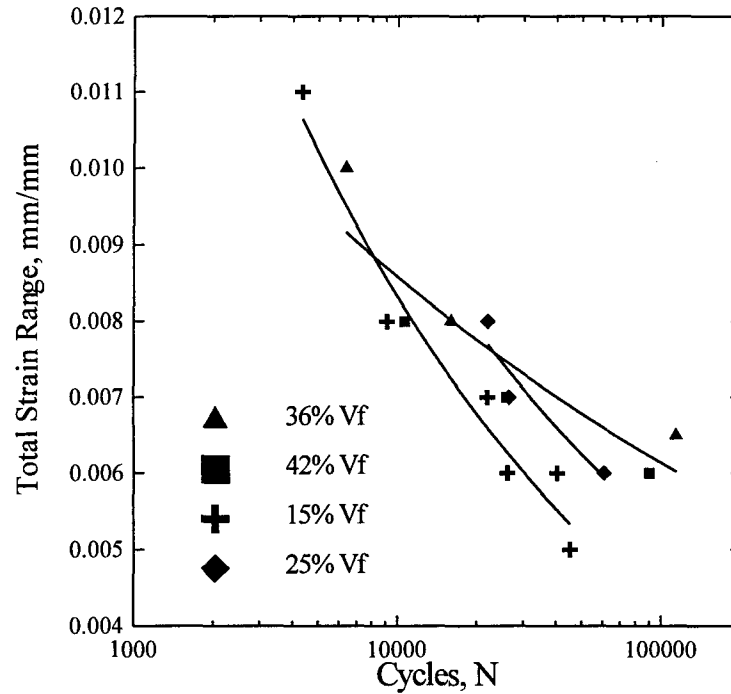


**Figure 24. S-N Diagram for all Fiber Volume Fractions**

The differences in fatigue life between the fiber volume fractions seen in Figure 24 are likely a result of the matrix fatigue behavior. Using the fatigue life regions shown in Figure 3 and the observed failure modes as discussed in Section 4.3 later, the data from this study is categorized into Region II of the S-N diagram. In this region the dominant damage mechanism is fiber bridged matrix cracking. This matrix fatigue behavior is different for the various fiber volume fractions. Because the lower  $V_f$  material has less

fiber reinforcement, fatigue cracks will propagate faster due to less crack tip shielding from fibers [7]. So the cracks grow faster and possibly allow for the growth of a dominant crack early in fatigue life. This is reinforced by the observation of fewer crack planes in the lower fiber volume fraction specimens, as discussed later in Section 4.3.

The matrix also affects specimen behavior through its load carrying capacity in the laminate. This capacity was analytically determined using a tool called LISOL. LISOL is a linear inelastic MMC micromechanical stress analysis solver package developed by Robertson [29]. This tool was used to find that the matrix carried over 72% of the applied load in the 15%  $V_f$  specimens, at an applied strain level of 0.003 mm/mm. The matrix only carried 27% of the applied load for the same test in the 42%  $V_f$ . These values are computed after 100 simulated cycles. This shows that fatigue life is more dependent upon fatigue of the fiber and fiber/matrix interface in the higher fiber volume fractions, because the matrix is not the important load carrier.

#### **4.2.1 Stress Control and Strain Control Comparison**

The majority of research on SCS-6/Ti-15-3 laminates has been performed under the load or stress control mode. This study allows for the direct comparison between the different control modes for fully-reversed fatigue. The use of a buckling guide as compared to testing expensive, thick laminates was also examined. Figure 25 shows the trend line for all fully-reversed testing on 36% and 42%  $V_f$  unidirectional SCS-6/Ti-15-3. Included are 36% fiber volume fraction,  $[0]_{32}$ , thick specimens and data obtained with the use of a buckling guide.

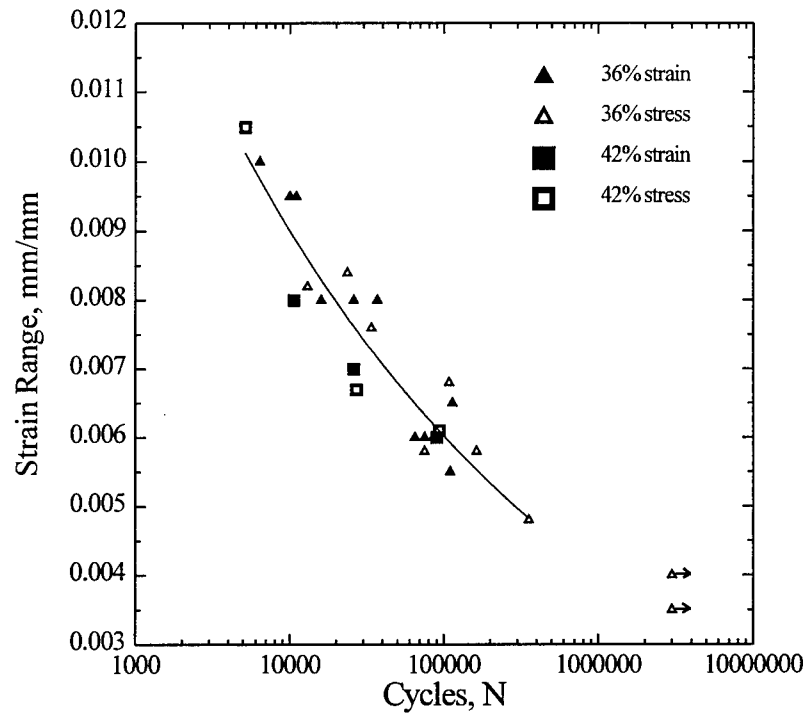


**Figure 25. S-N Diagram for High  $V_f$  Under Stress and Strain Control**

There is no significant difference in fatigue life between these two high fiber volume fractions and there is no discernable effect of the control mode. This supports previous conclusions based on the strain-control testing. Also, there is no apparent difference between the thin and thick composites, i.e. thickness effect or buckling. Given the difficulty and cost of the thick laminate fabrication, the use of a buckling guide has proven effective. In Figure 26, the 15%  $V_f$  data are added to the S-N diagram for both stress and strain control. There is an increasing difference in fatigue life as the applied strain range decreases. At higher strain ranges the fatigue life between fiber volume fractions is the same while the 15%  $V_f$  experiences significantly shorter life at strain ranges below 0.007 mm/mm.

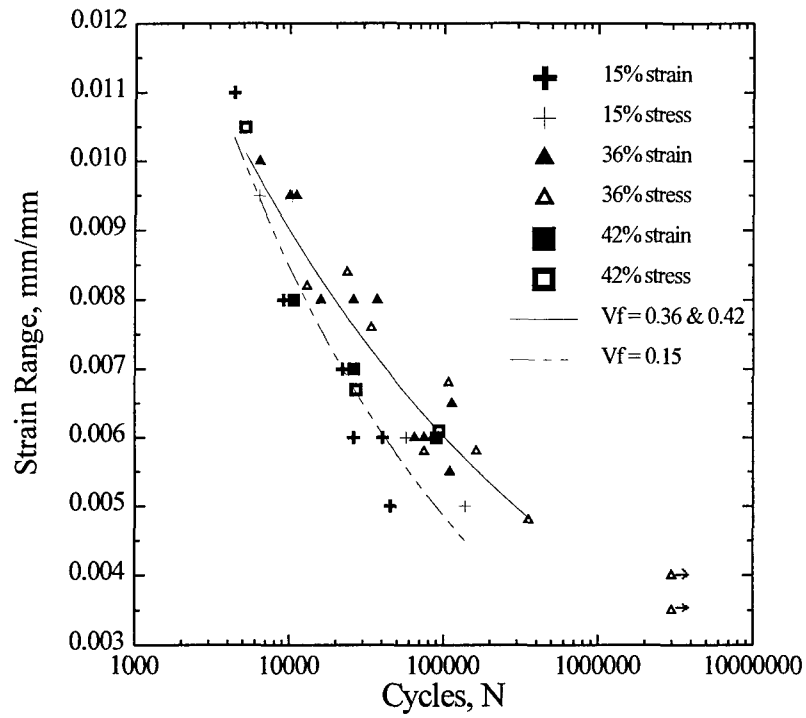


**Figure 26. S-N Diagram for all data except 25%  $V_f$**

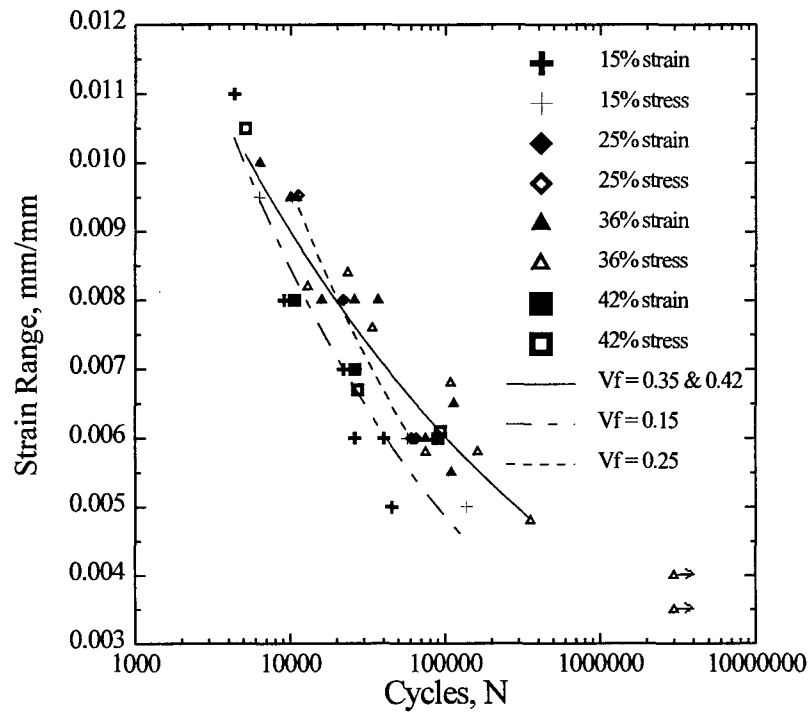


**Figure 27. S-N Diagram for all  $V_f$  and Control Modes**

The complete S-N diagram is shown in Figure 27. This includes the data obtained on the 25% fiber volume fraction, which falls in between the fatigue lives of the higher and lower fiber volume fraction data, as expected.

Clearly there is a fatigue life dependence on fiber volume fraction of the TMC at applied strain ranges at and below 0.008 mm/mm. Fatigue lives increase with an increase in fiber content. Though the 36%  $V_f$  and 42%  $V_f$  are close in fiber content, the similarity in fatigue life possibly indicates a threshold of no more benefit to adding more fibers. A non-destructive evaluation of the 42%  $V_f$  material prior to machining indicated problems with cross-weave consolidation and the fiber/matrix interface. Fiber alignment and spacing were not as good as in the other laminates. These material deficiencies were assumed to be so minor as to have little effect on the study, since the data presented here show the 42% fiber volume fraction to have practically the same life as that of the 36%  $V_f$  as expected.

A closer inspection of the 15%  $V_f$  data shows a minor difference between the control mode of the tests. For ease of study, the data is shown separately in Figure 28. The tests performed under stress control have a longer fatigue life than that under strain control, while the trend is identical in both modes. The likely cause of this difference is related to the matrix content in the material. The hardening characteristics of the matrix and the significant role it plays in carrying the specimen load for this fiber volume fraction has been previously discussed. As the specimen hardens, or becomes stiffer, more load is applied to maintain strain range in strain control. This leads to earlier crack initiation and faster crack growth. Therefore a reduced fatigue life is produced in

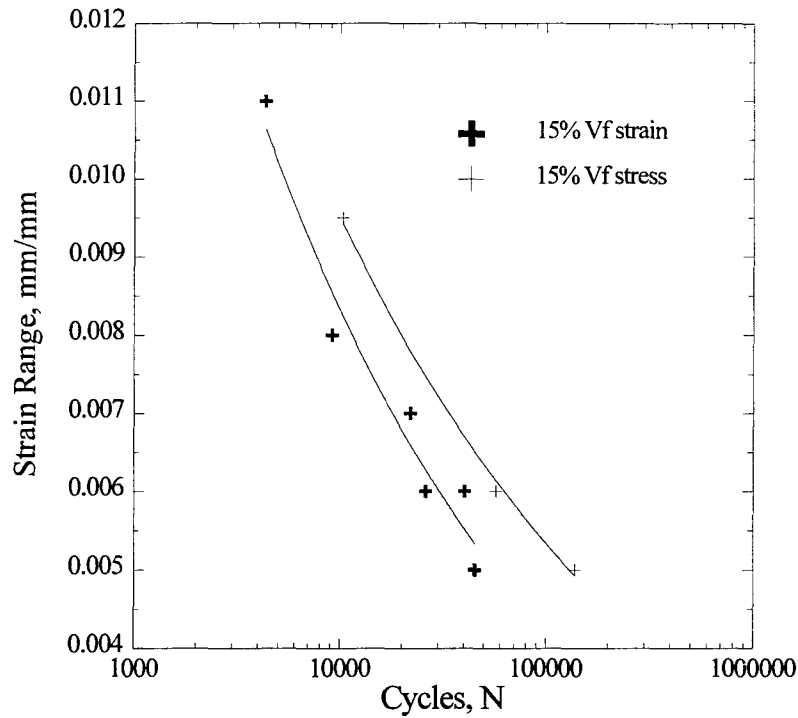


**Figure 25. S-N Diagram for 15%  $V_f$  Stress and Strain Control**

comparison to a stress-controlled test. In a stress-controlled test, the strain range is free to decrease as hardening occurs, thus slowing the damage rate in the material. The effect is not observed in the other fiber volume fractions due to the reduced load sharing of the matrix material. Other studies involving higher fiber content material show no difference in the control mode [14,18].

The use of the AFIT buckling guide appears to have had no effect on the data obtained in the study. The thick ply material data [18] compares favorably to the anti-buckling guide data, therefore no distinction has been made between the data.

#### 4.2.2 Fiber Stress Analysis

Previous study has shown composite life for different lay-ups to be controlled by the  $[0]$  ply fiber stresses [28]. The fiber stress calculations for the tests completed in this study were performed using a program by Robertson called LISOL [29]. This micromechanical analysis program allows the user to account for residual stresses in the laminate from processing in the HIP and ramp-up to test temperature. The results are shown in Figure 29, including data from Jackson who tested a 36%  $V_f [0^\circ]_8$  laminate with a buckling guide under strain control. This figure plots the fiber stress versus cycles to failure for all  $V_f$ . These data are identical to the S-N diagrams based on strain range. The 15%  $V_f$  data has slightly shorter fatigue lives than other  $V_f$  data, while there is a greater difference in life between different  $V_f$  at the fiber stress ranges below 2400 MPa. The 25%  $V_f$  data shows a relatively high fiber stress range for one test and the 36%  $V_f$  has a higher life for all stress ranges.

The most important point from Figure 29 is that fiber stress data from different  $V_f$  do not collapse into one curve which would indicate that fatigue life is dominated by stresses in the fiber. Thus it is shown that matrix response is also important in determining cycles to failure.

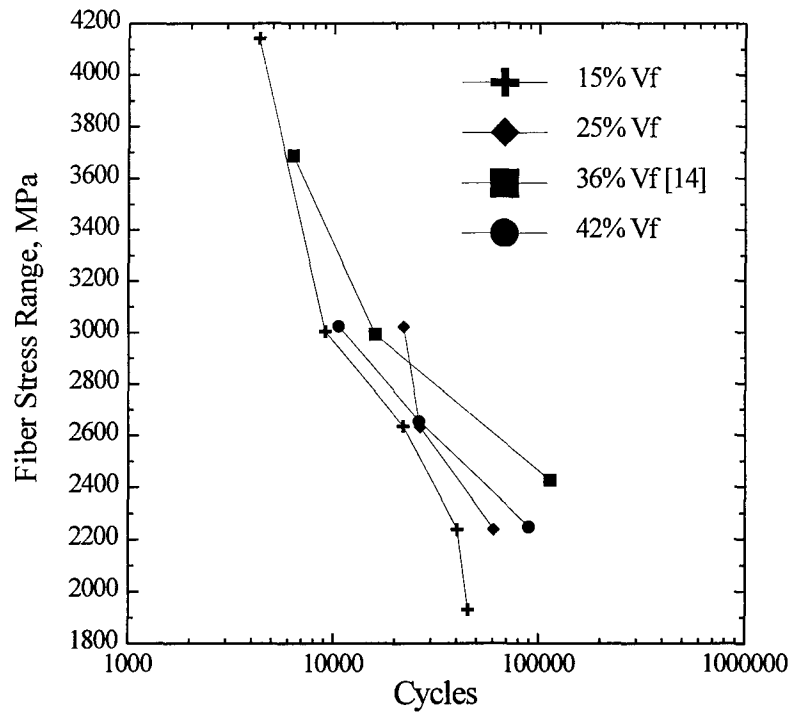


**Figure 29. Fiber Stress Range versus Cycles for all Fiber Volume Fractions**



### **4.3 Microscopic Analysis**

Damage mechanisms for fatigue have been documented in many previous studies for tension-tension fatigue testing of TMCs. Kraabel [17] and Jackson [14] concluded that there is little difference in damage mechanisms for tension-compression and tension-tension testing. These damage mechanisms include matrix cracking, fiber/matrix interface cracking, and environmental effects. One mechanism found unique to fully-reversed testing is the debonding of the interface between matrix foil layers used for manufacture due to the compressive loading. Because this study has a focus on the effects of fiber volume, close attention will be given to damage mechanisms related to fiber spacing and foil thickness. The quantity of matrix cracking, the effect of the different cross-weave materials, and amount of material ruptured during failure will also be looked into to provide a complete microscopic analysis of the fracture surfaces.

#### **4.3.1 15% Fiber Volume Fraction**

The major damage mechanism during fatigue is the initiation and propagation of cracks in the material perpendicular to the applied load. Crack initiation sites for this SCS-6/Ti-5-3 laminate are any type of material irregularity. These include processing flaws, the Mo cross-weave, specimen edge imperfections, and the fiber/matrix interface. The Mo cross-weave can be seen in Figure 30, where it appears as a wavy ribbon warping between the fibers seen in a head on view. The cross-weave has a dominant presence on this portion of the fracture surface. Once a crack has initiated, it has been shown that it will grow faster in this low 15% fiber volume fraction due to less fiber reinforcement of the advancing crack tip [7].

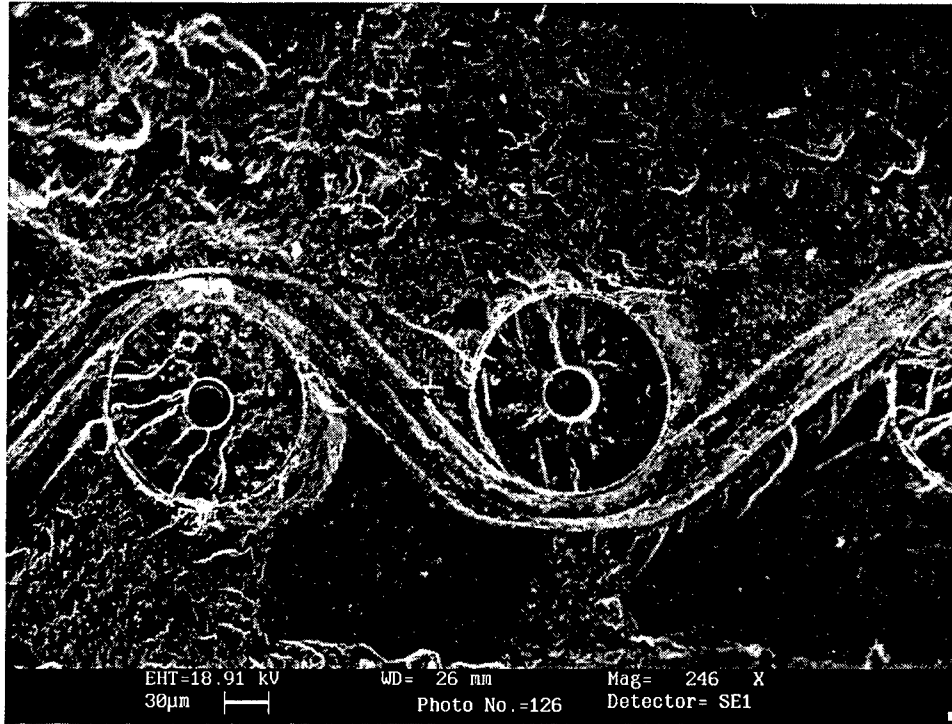


**Figure 30. Molybdenum Cross-Weave on the Fracture Surface**

As previously discussed, the amount of fatigue cracking increases with decreasing values of applied strain according to the modulus behavior. This can be observed in Figure 31, where fatigue cracking dominates 70% of the fracture surface for a specimen tested at 0.25% maximum strain. The fatigued area is characterized by a relatively flat surface with little highlights from voids. Also, the fatigued surface is definable by the formation of oxide, which is the result of a reaction of the material with air that infiltrates the crack as it advances. The high temperature of this study increases the reactivity rate and oxidation occurs quickly. In Figure 31 the fatigued portion of the surface is approximately the right two-thirds of the specimen. Note the Mo cross-weave on the upper portion of the fracture surface.

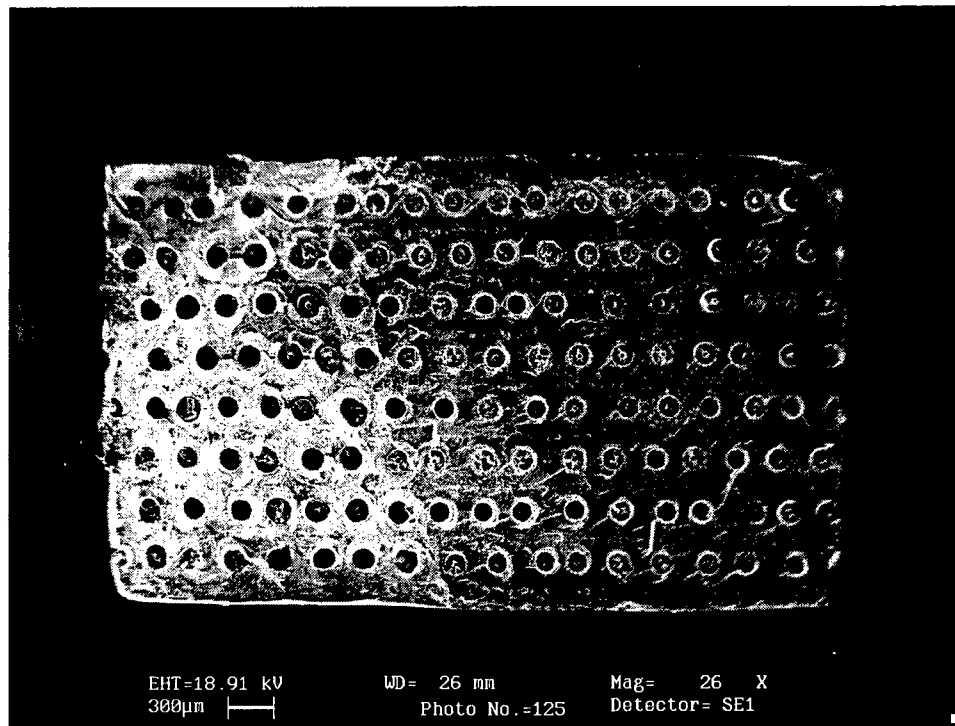


**Figure 31. 0.0025 mm/mm 15%  $V_f$  Specimen Fracture Surface**

Figure 32 shows the fracture surface of the 0.55% maximum strain test, which is fatigue cracked over only 45% of its surface. Location of the fatigue cracks is also important. Examination of Figure 32 shows a fracture surface with a large matrix crack on a single plane. On comparison of this to Figure 33, showing the fracture surface of a specimen tested at 0.35% maximum strain, and then to Figure 31, it is seen that higher applied strain produces fracture with fatigue cracks located on many different planes. One similarity in all specimens was the eventual formation of a dominant fatigue crack. This is the crack that ultimately causes failure and was located on a specimen corner, rather than the interior, for all tests.

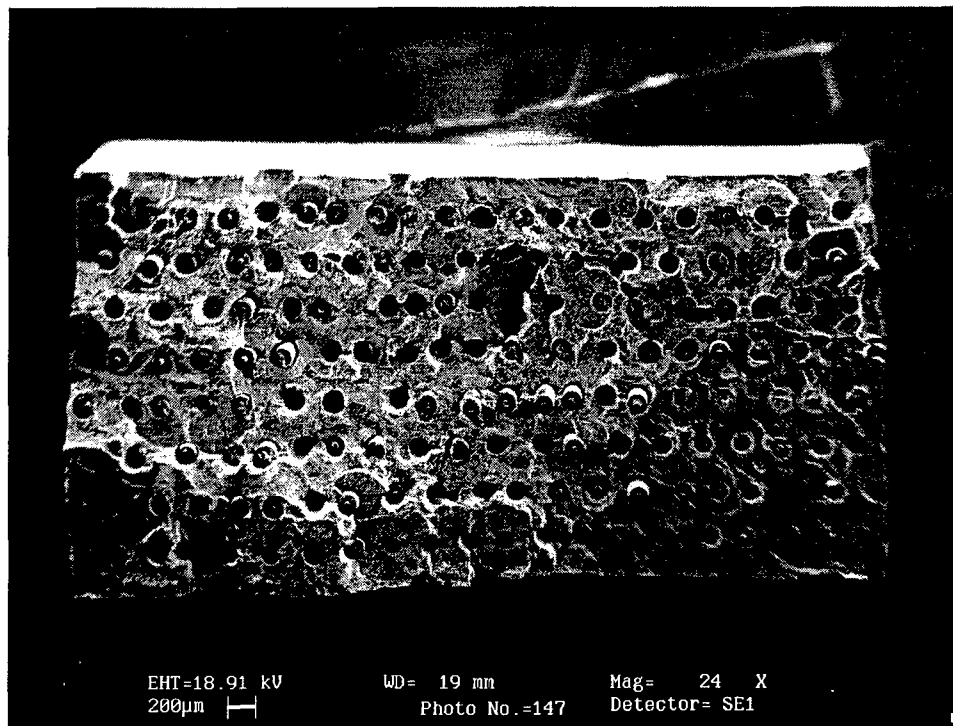


**Figure 32. 0.0055 mm/mm 15%  $V_f$  Specimen Fracture Surface**

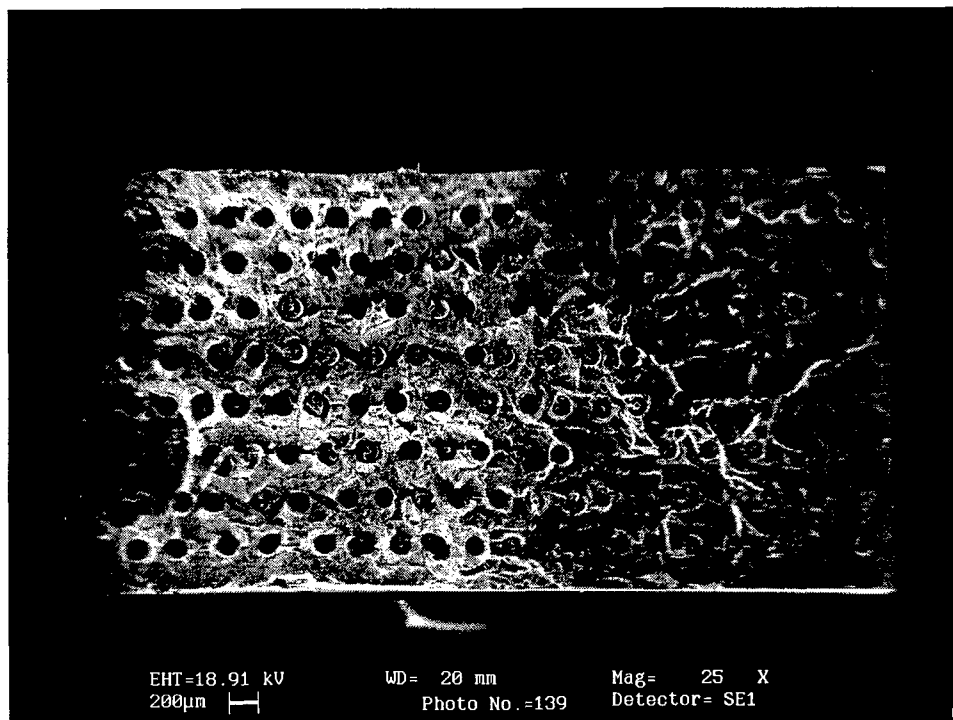


**Figure 33. 0.0035 mm/mm 15%  $V_f$  Specimen Fracture Surface**

Tensile failure is characterized by fiber pullout and matrix rupture, shown in Figure 34. The dimples in the matrix are formed by necking when the matrix is subjected to local overload. Since silicon carbide fibers do not yield, once the critical load or stress is reached the fibers fail catastrophically and the remaining matrix is overloaded. All specimens exhibited this failure mechanism in the areas where there was no fatigue cracking, thus indicating that these failed during the tensile portion of fatigue loading. Note the Mo cross-weave present in Figure 34. Even in a tensile failure region, there may be preferential failure occurring around this irregularity.

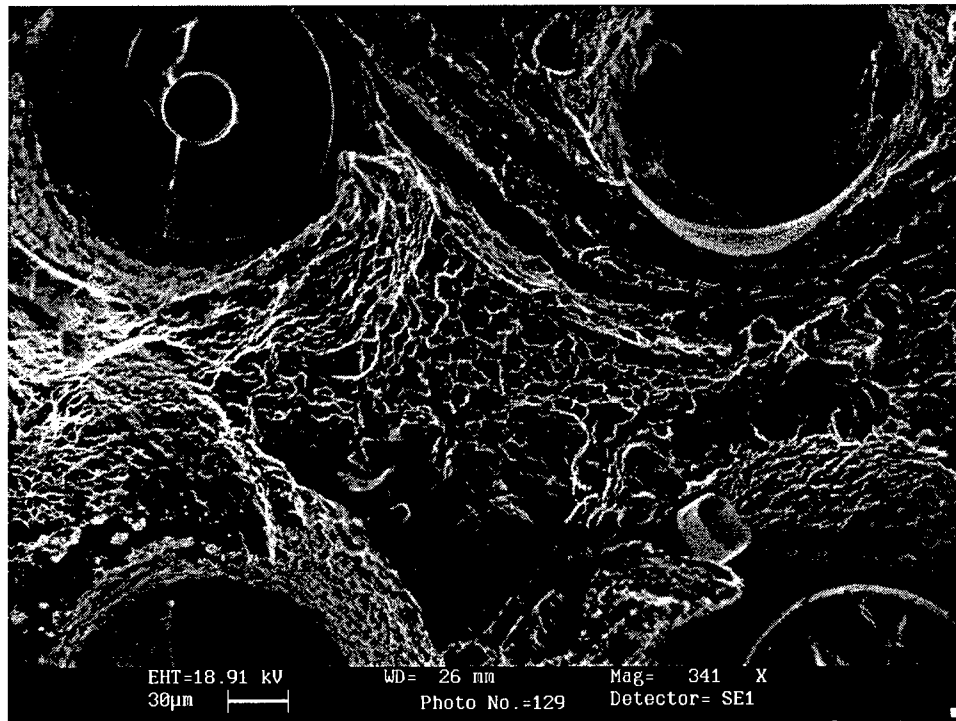


**Figure 34. Ductile Rupture Matrix Dimples**

There are other damage mechanisms that depend on strain range. The foil/foil interface, shown in Figure 35, was much more important in the higher strain range, low  $V_f$  specimens. In this micrograph the interface has delaminated and is visible between the cylindrical fibers at many locations. Crack planes are often connected by these delaminations. The lower strain ranges showed little affect from the foil interface damage.

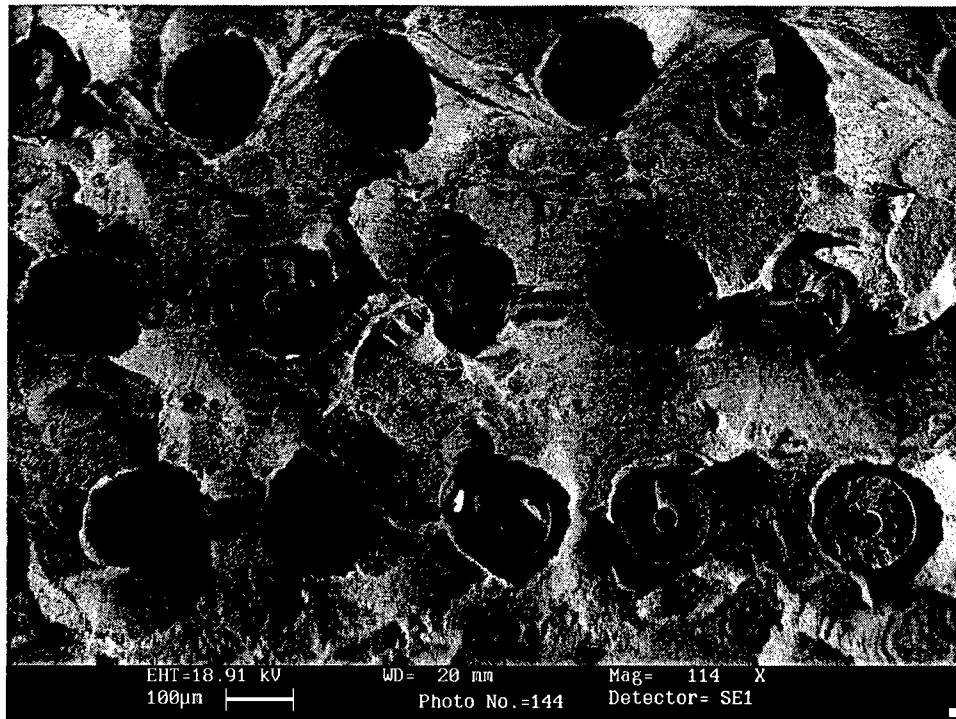


**Figure 35. 0.0035 mm/mm 15%  $V_f$  Specimen Fracture Surface**

The molybdenum cross-weave also proved more detrimental to the low applied strain tests, appearing with greater frequency on the fracture surface. The tests performed at strain levels of 0.004 mm/mm and 0.0055 mm/mm show only minor influence of the

cross-weave on fatigue cracking. Cracking was also observed in the specimens away from the fracture surface. These cracks become more numerous with increasing applied strain range, and none were observed in the specimens tested at 0.35% strain or below. One example of this fatigue cracking can be seen in Figure 36, where the maximum applied strain was 0.55%.

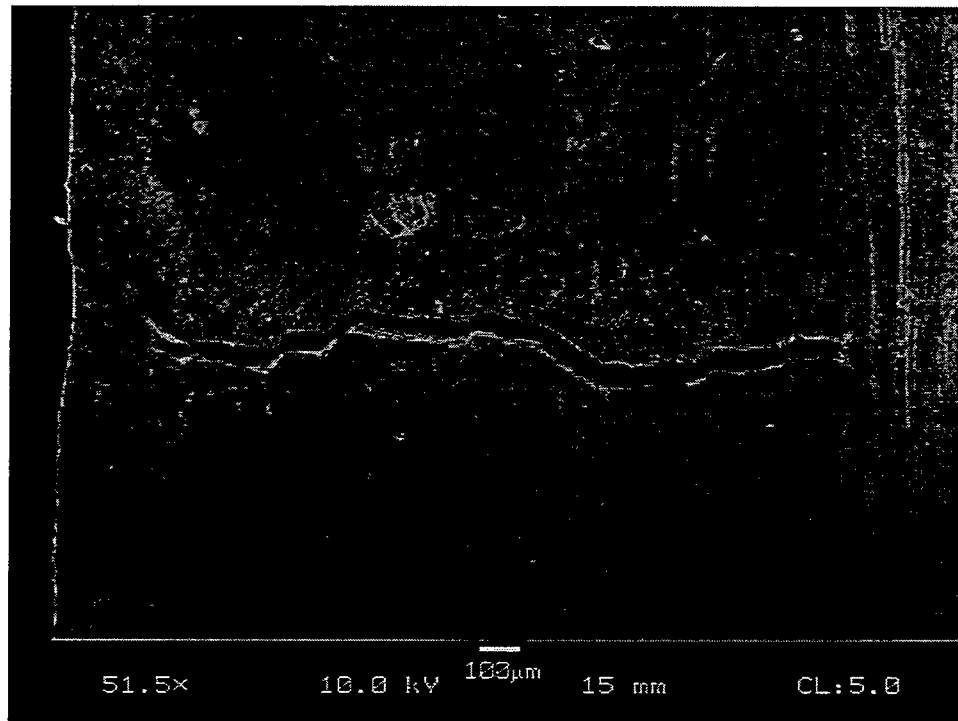


**Figure 36. 0.0055 mm/mm Specimen Face Away From Fracture Surface**

A new feature of failure was examined on the fracture surfaces of the 15%  $V_f$  material. Large dimples in the tensile rupture regions were found at the interface of the matrix foil layers, like the one shown in Figure 37. A monotonic tensile test, performed subsequent to this observation, yielded the same feature, thereby excluding any

compressive buckling damage mechanism as the cause. Because of the size and location, these dimples are thought to be processing flaws due to incomplete consolidation of the material from utilization of thicker matrix foils.

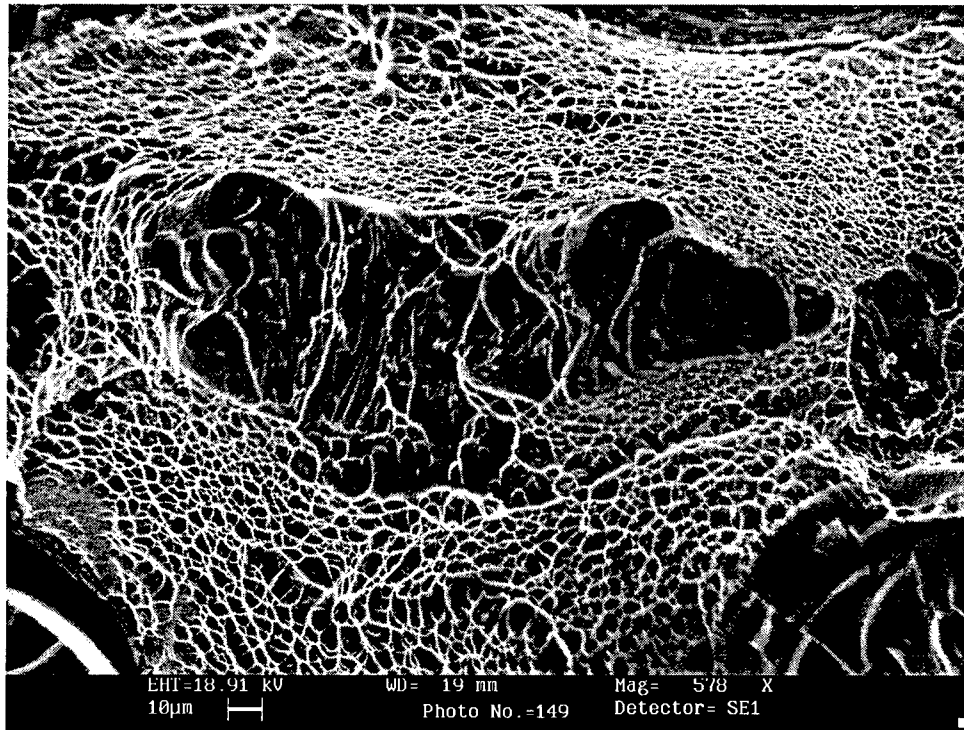


**Figure 37. Large Dimples on Matrix/Matrix Interface**

#### **4.3.2 25% Fiber Volume Fraction**

The damage mechanisms for the 25%  $V_f$  specimens are the same as the 15%  $V_f$  with the exception of the cross-weave interactions. The 25%  $V_f$  material has a titanium/niobium wire as the cross-weave material. Unlike the 15%  $V_f$  material, this cross-weave was not found to be the cause of any damage on the fracture surface. No Ti-Nb material was noted on any of the fracture surfaces, which means it is not a crack



initiation site like the molybdenum cross-weave. Because of the smaller variation in strain range covered by these tests, only 0.006 mm/mm to 0.008 mm/mm, all the fracture surfaces exhibited similar properties. The amount of fatigue cracking on all fracture surfaces was between 60% and 80%.

The test performed at a maximum strain of 0.3% is shown in Figure 38 and is typical of all three tests performed. Matrix cracking covers about 65% of the fracture surface, contained in three crack planes which are connected by delaminations along the fiber/matrix foil interface line.

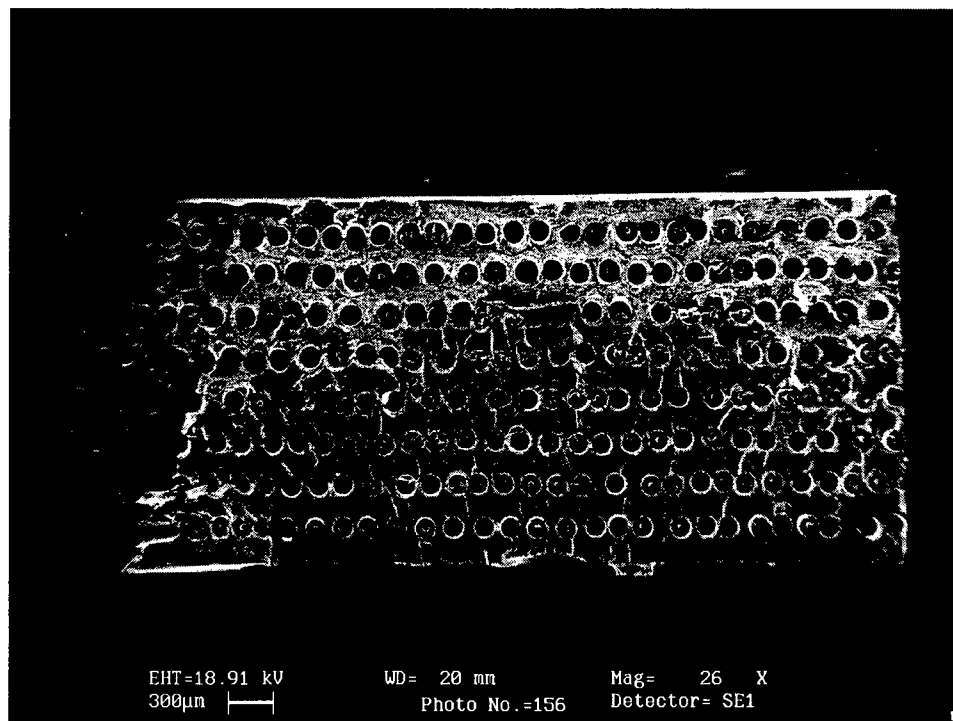


**Figure 38. 0.003 mm/mm 25%  $V_f$  Specimen Fracture Surface**

Figure 39 shows the fracture surface of the specimen tested at a maximum strain level of 0.4%. This micrograph is a good example of a delamination along a row of fibers connecting two crack planes. A side view of this same specimen is shown in Figure 40. A micrograph of the 0.35% maximum strain specimen is shown in Figure 41. Here the amount of matrix cracking is approximately 80%. The trend of increasing number of crack planes with increasing applied strain is not seen in the 25%  $V_f$  data. The likely explanation is the small variation in strain range that was investigated.

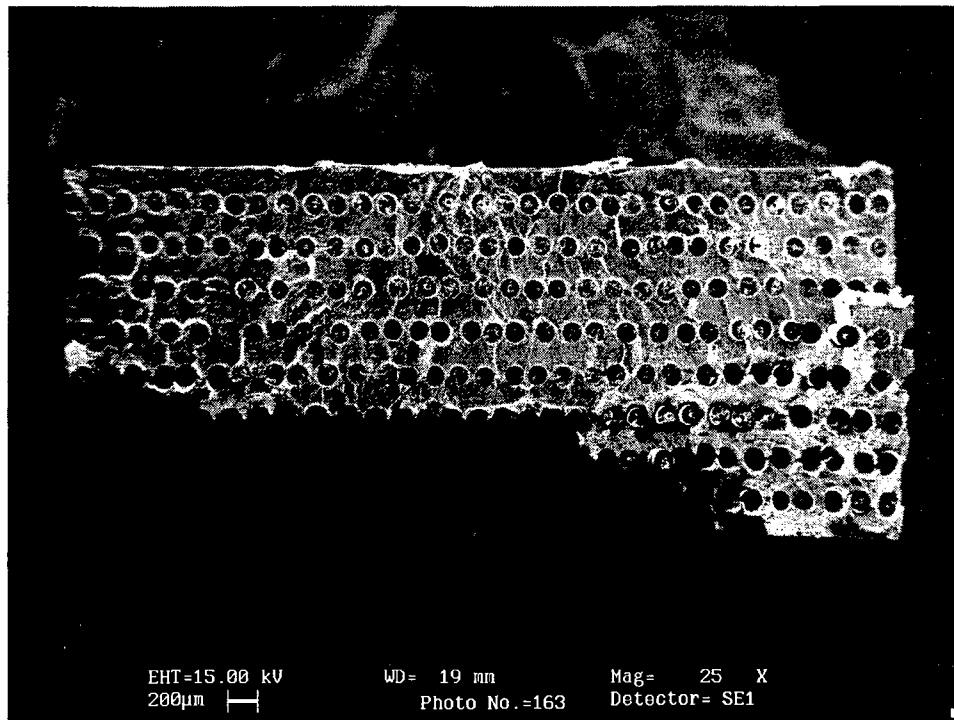


**Figure 39. 0.004 mm/mm 25%  $V_f$  Specimen Fracture Surface**

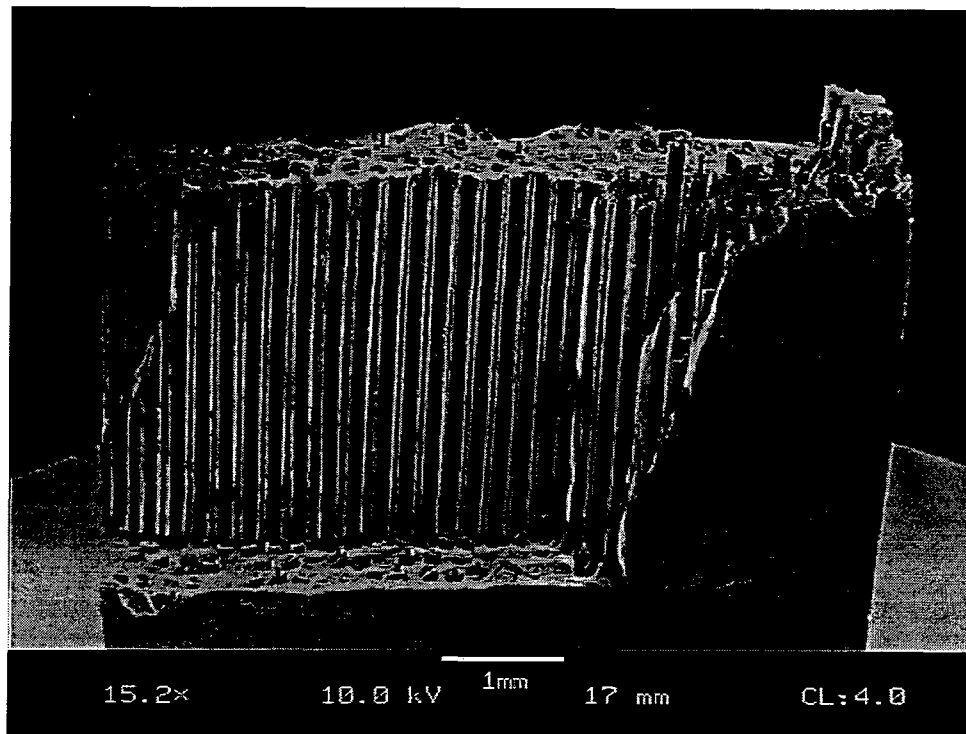


**Figure 40. Side view of 0.004 mm/mm 25%  $V_f$  Specimen**

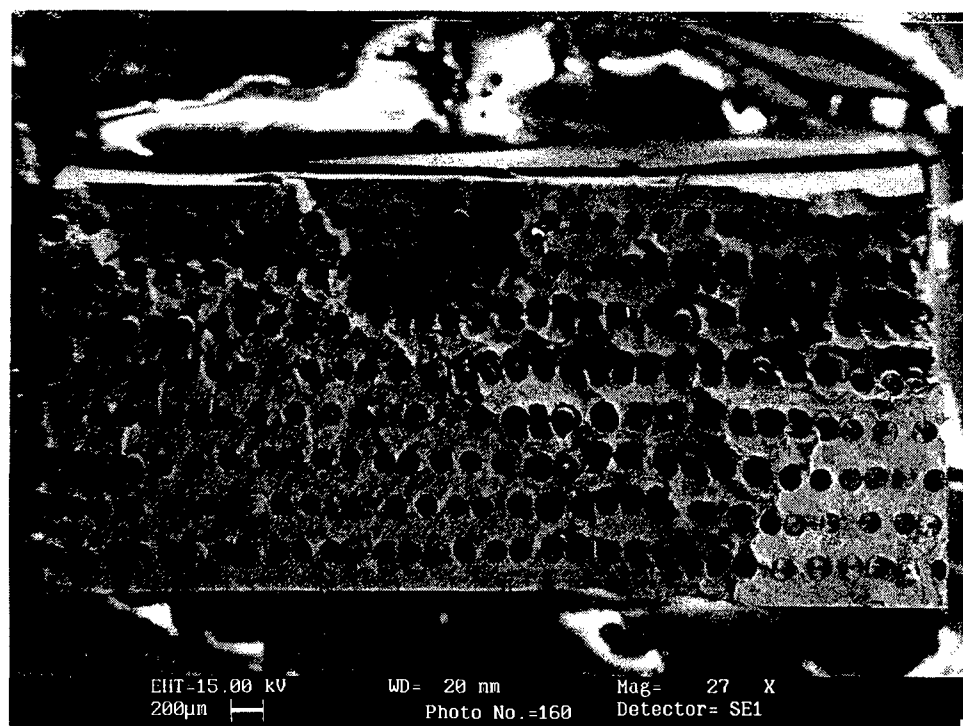


**Figure 41. 0.0035 mm/mm 25%  $V_f$  Specimen Fracture Surface**

The compressive damage manifested in delamination of the foil/foil interface was much less apparent in the 25%  $V_f$  specimens. Though in some locations the crack planes were joined by large delaminations along the fibers, there were few locations on the fracture surfaces themselves. The large dimples found along the foil/foil interface in the 15%  $V_f$  specimens were present in the 25%  $V_f$ , but in smaller amounts. These differences between  $V_f$  may be caused by the change in fiber spacing, the reduction of the load that the matrix carries, or the change in matrix foil thickness. Damage away from the fracture surface was limited only to the specimen tested at a maximum strain of 0.4%. It exhibited fiber fracture on the same plane extended from the fracture surface crack, shown in Figure 42. This micrograph is of the face of the specimen just outside the fracture, polished down to reveal the first fiber layer.

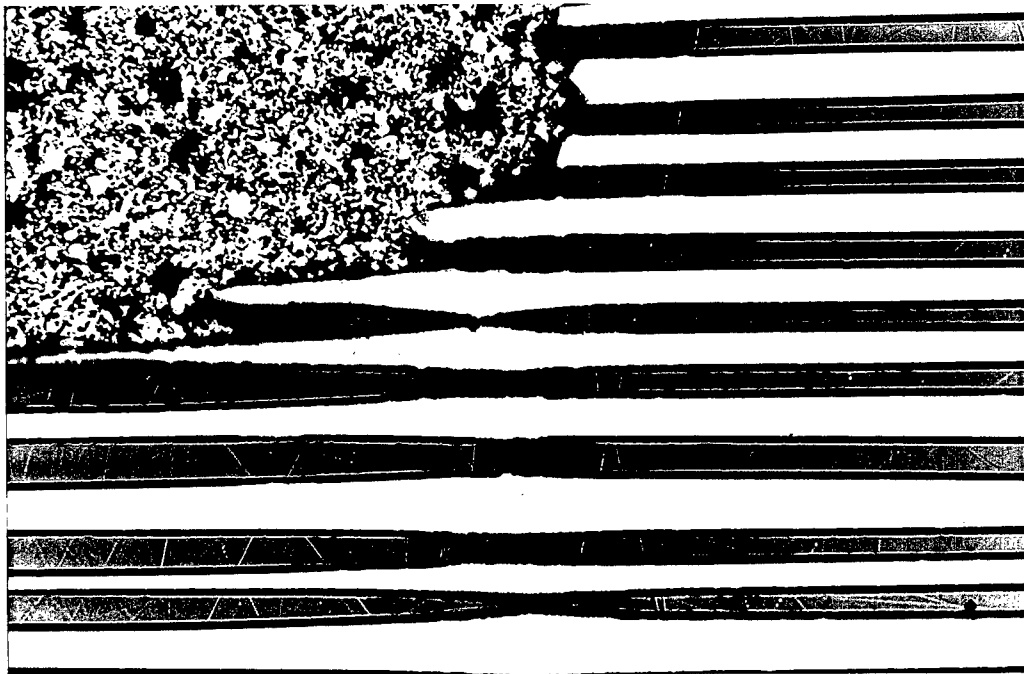


**Figure 42. Fractured Fibers Ahead of the Crack Tip (5X)**

There were also some small matrix edge cracks that were approximately five fiber layers deep, as a representative micrograph shows in Figure 43. These cracks have bridged, or passed around, the fiber and continue propagating without breaking the fiber. A detail of a bridged fiber is shown in Figure 44. The other two strain level specimens showed no damage in the gage section of the specimen away from the fracture surface. The polished face appears undamaged as in Figure 45. This data supports the observation that there is more cracking away from the fracture surface in the higher strain range tests.

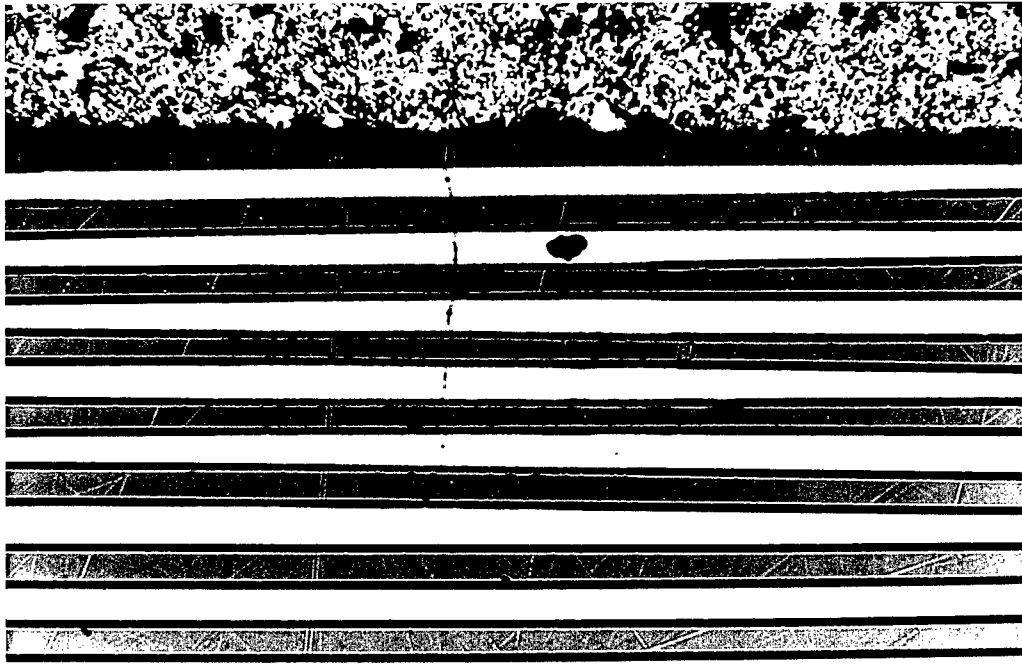


**Figure 43. Matrix Crack on Specimen Edge, 0.8% Strain Range (5X)**

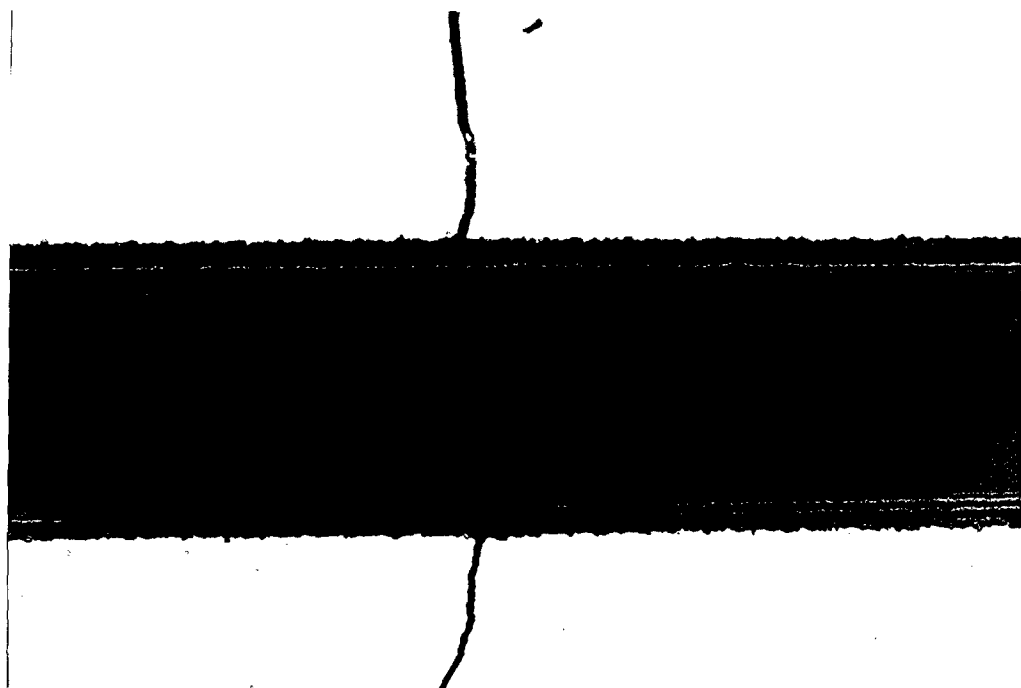


**Figure 44. Fiber Bridged Matrix Crack (40X)**

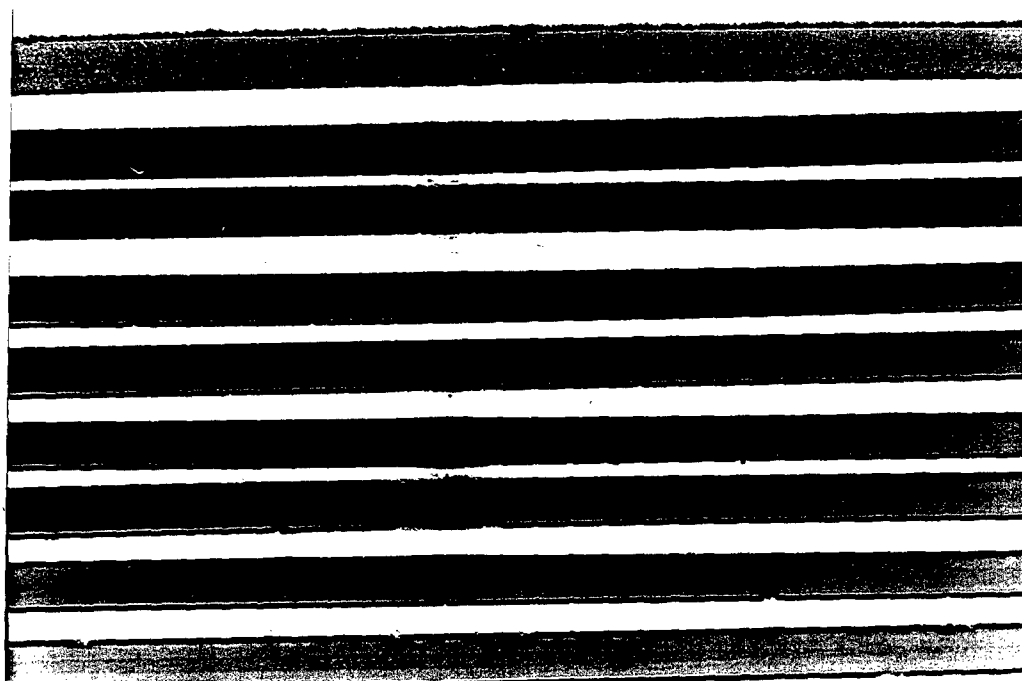


**Figure 45. Undamaged Specimen Face in Gage Length, 0.7% Strain(5X)**

### 4.3.3 42% Fiber Volume Fraction

Figure 46 shows the fracture surface of the test performed at a maximum applied strain of 0.004 mm/mm. Approximately 85% of the fracture surface is dominated by the fatigue crack damage mechanism. One interesting observation is that the cracking has manifested itself in six different crack planes, more than seen in the previous two fiber volume fraction specimens. Shown in Figure 47 is the fracture surface of the test performed at 0.3% strain. There are fewer crack planes in this specimen, but still a high number compared to the other  $V_f$ . Figure 48 shows the fracture surface for the specimen tested at 0.35% maximum strain.

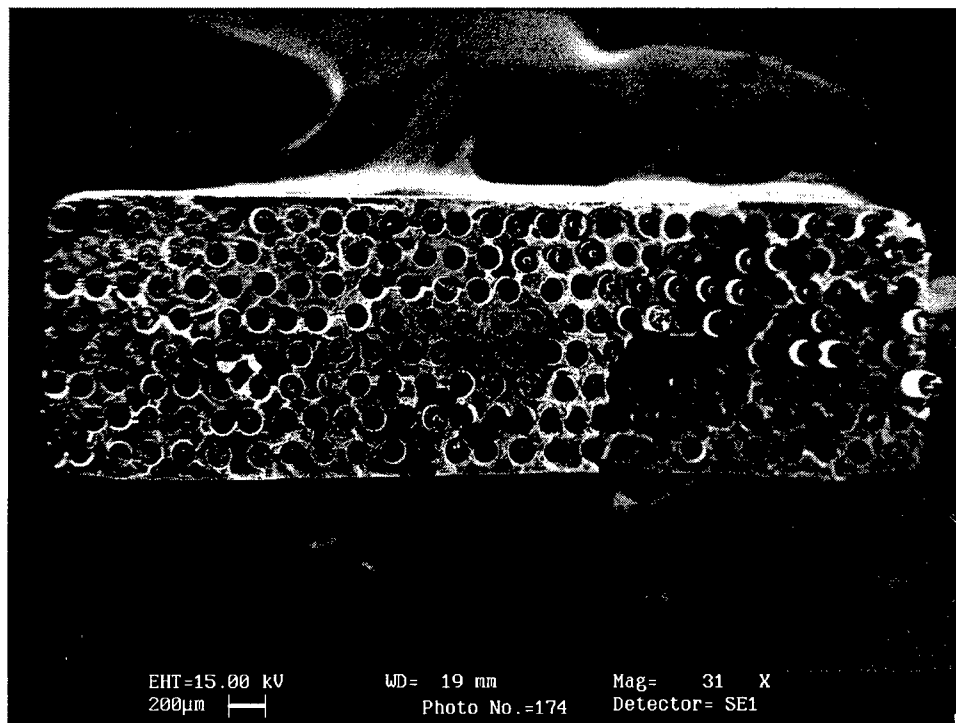


**Figure 46. 0.004 mm/mm Specimen Fracture Surface**

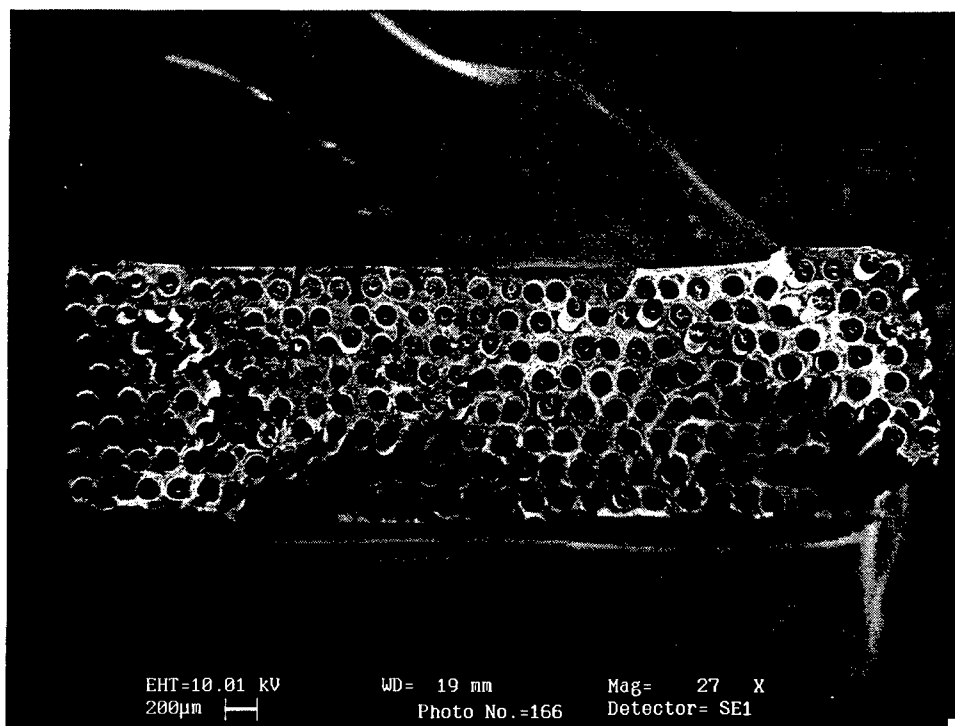


**Figure 47. 0.003 mm/mm Specimen Fracture Surface**

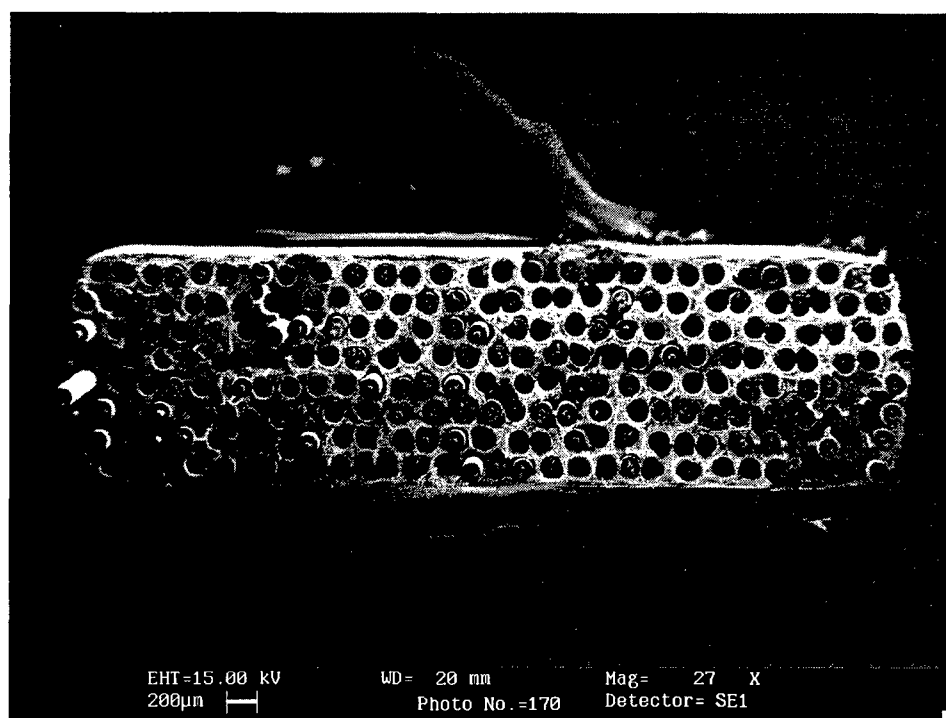


**Figure 48. 0.0035 mm/mm Specimen Fracture Surface**



Fracture surfaces for the 42%  $V_f$  contain the same damage mechanisms as seen previously, but the damage is on many more crack planes. The likely cause for this behavior is the increased number of crack initiation sites with the large number of fibers in the specimen. There is much more fiber/matrix interfacial area as well as decreased fiber spacing in this fiber volume fraction. From comparison of these three 42%  $V_f$  fracture surfaces shown, it is concluded that there is no clear relation between applied maximum strain and amount of crack damage. Figure 47 shows a fracture surface with at least 6 distinct crack planes and was tested at a low strain of 0.3%. The 0.4% strain specimen shown in Figure 46 has the same number. The minor variation in applied strain is the cause for this difference.

This fiber volume fraction also contained the molybdenum cross-weave material for fiber alignment during consolidation. This Mo cross-weave is present on every fracture surface and nearly every crack plane for the 42%  $V_f$ , indicating what a strong matrix fatigue crack initiation site it is. Figures 49 and 50 show this effect. Figure 49 shows three fibers that have been fractured and matrix that is cracked from the inclusion of the Mo cross-weave. Under high optical magnification, the damage to the matrix and the fiber/matrix interface can be clearly seen in Figure 50.

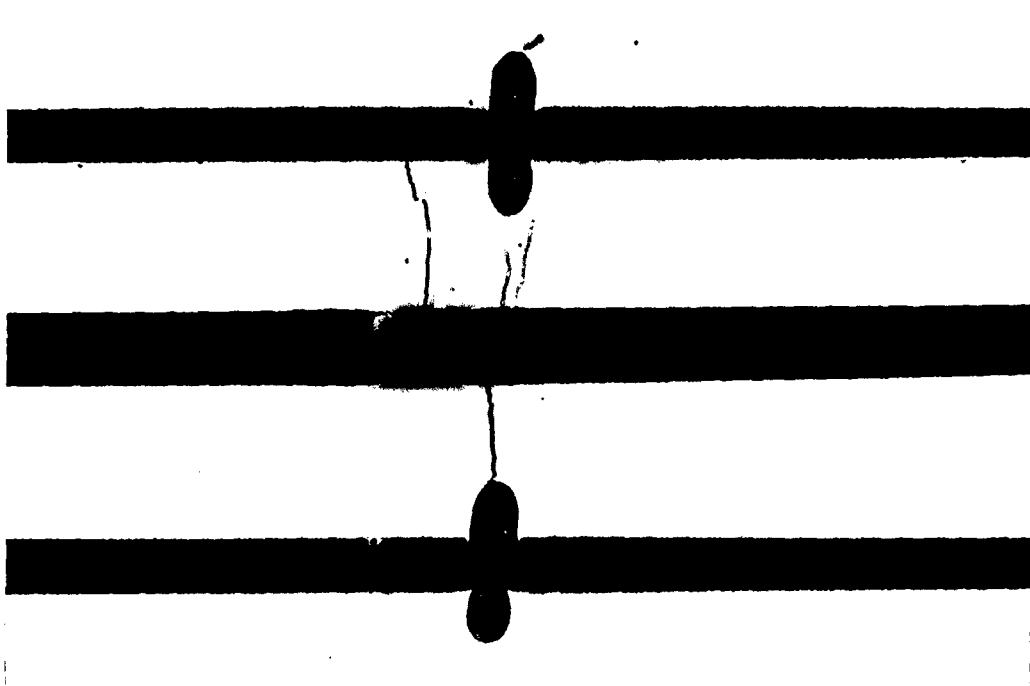


**Figure 49. Damage Initiated From Mo Cross-Weave (10X)**

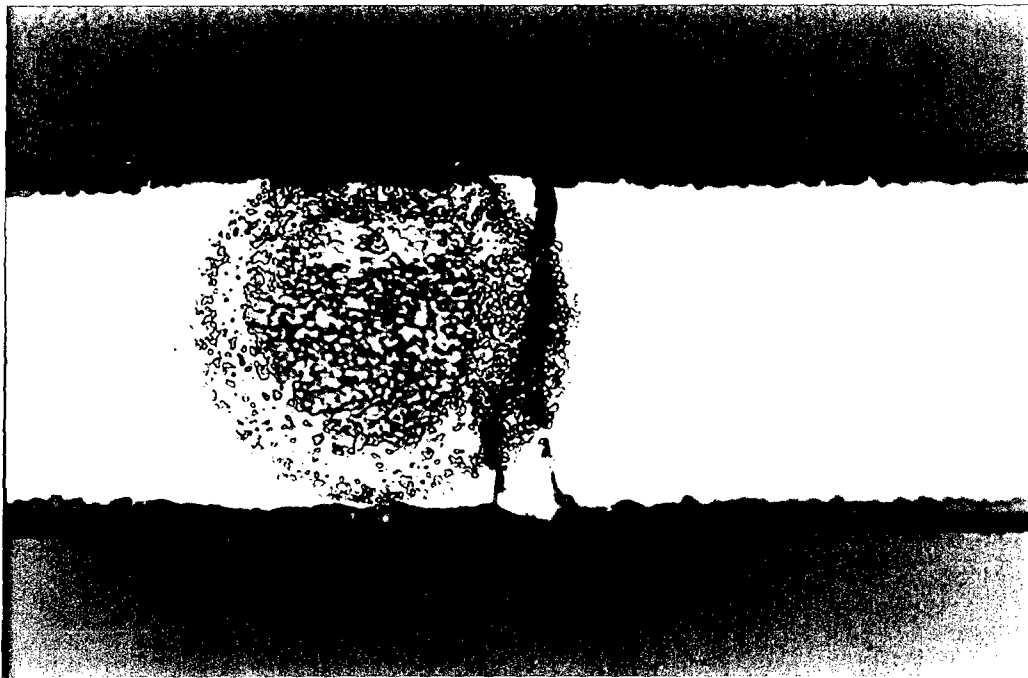


**Figure 50. Fiber/Matrix Interface Damage at Mo Cross-Weave (100X)**

Compressive damage mechanisms were not nearly as prevalent as in the other fiber volume fractions, indicating a decrease in compressive matrix damage with an increase in  $V_f$ . Very few of the large dimples on the matrix/matrix foil interface were observed, and delaminations were limited to joining adjacent crack planes. Because the delaminations occurred along the fiber rows and not at the matrix/matrix foil interface, it is likely that this damage mechanism is related to fiber spacing and not matrix foil thickness.

## 5. Summary and Conclusions

The purpose of this study was to identify the effects of fiber volume fraction,  $V_f$ , on the fatigue response of a unidirectional, SCS-6/Ti-15-3 TMC laminate at 427°C. The damage mechanisms and fatigue life were investigated for fiber volume fractions of 15%, 25%, and 42% and compared with 36%  $V_f$  data obtained in previous studies [14,17,18]. The fatigue condition involved a fully-reversed,  $R_g = -1.0$ , strain controlled triangular waveform loading. A single neat matrix test was also performed to gain insight into the fatigue behavior of the matrix. Further, micromechanical analysis was conducted to understand how the fatigue behavior may be affected by various amounts of fiber and matrix constituents.

For all fiber volume fractions, similar damage mechanisms were observed that concurred with findings of previous studies [14,17,18]. At applied maximum strain levels of 0.0055 mm/mm or greater, there was significant fiber pullout and tensile rupture of the matrix. Matrix fatigue cracking was a minor characteristic on the fracture surface. However, at applied strain levels below 0.0055 mm/mm, matrix fatigue cracking was the dominant feature of the fracture surfaces for all fiber volume fractions. The main difference in fracture surfaces was not the percentage of fatigue cracked surface but the number of crack planes that formed and coalesced before failure. The 42%  $V_f$  fracture surfaces had many crack planes while the low 15% fiber volume fraction had very few. This is mainly attributed to the numerous crack initiation sites in the 42%  $V_f$  laminate. Typically in the 15%  $V_f$  laminate, a single dominant crack plane would develop which lead directly to failure. These matrix crack dominated failure modes were observed in

previous studies for both fully-reversed stress- and strain-control modes. Thus it is shown that damage mechanisms are the same regardless of control mode or fiber volume fraction.

The secant modulus response of the SCS-6/Ti-15-3 material showed a trend of increasing degradation with increasing applied maximum strain. Key factors in this behavior are the competing mechanisms of matrix hardening and fatigue cracking. Matrix fatigue cracking causes the modulus to decrease while strain hardening makes the material stiffer. The higher maximum applied strain tests have a more rapid crack initiation and growth, thus a larger modulus degradation. The lower applied strain tests have a longer test duration, leading to more phase precipitation hardening of the matrix than the higher strain tests, as well as slower crack initiation and growth given by the longer fatigue lives. Because of the matrix-oriented strain hardening, the lower fiber volume fractions with more matrix material are strongly affected by this behavior. In summary, material stiffness decreases in fatigue as fiber volume fraction and applied maximum strain increase. The propagation of matrix fatigue cracks in the different fiber volume fractions is evident in the fatigue life diagrams.

Fatigue life of the  $[0]_8$ , SCS-6/Ti-15-3 material can be examined using several parameters. On an applied strain range ( $\Delta\epsilon$ ) basis, the material showed similar fatigue lives at strain ranges of 0.007 mm/mm and above. Below this level, there was an increase in fatigue life with increasing fiber volume fraction. On a fiber stress range basis, the fatigue life was very similar to the  $\epsilon$ -N curve. The data followed the same trends, and revealed that life is affected by more than simply the stress in the  $0^\circ$  fibers. This indicates

that the matrix affects fatigue life, agreeing with the conclusion drawn previously about the influence of the matrix on the modulus history. When the fatigue life is looked at in terms of a Talreja diagram, the data developed in this study falls into the lower portion of Region II. In this region, failure is dominated by matrix cracking in the material. Fatigue life beyond 100,000 cycles was not studied so Region III, the fatigue limit of the material, was not covered in this research.

The affect of control mode on the fatigue life was also examined for this data. It was found that load- or stress-controlled data had slightly higher fatigue life than the strain-controlled data in the 15%  $V_f$  TMC. This is because of the hardening characteristic of the matrix and the large percentage of the load it carries in this low  $V_f$  material. No significant difference was observed between control modes in the higher  $V_f$  TMC, which agrees with previous study conclusions [14].

The use of a cross-weave material during consolidation of the TMC provided another parameter for comparison. The 25%  $V_f$  TMC had a titanium-niobium wire to hold the fibers in alignment while processing. This material has proven much more effective than the molybdenum used in the other  $V_f$ . The Mo cross-weave was present on almost all of the fracture surfaces of the 15% and 42%  $V_f$  specimens. This had a direct impact on the fatigue life while the Ti-Nb reinforcement was never observed, and is thus a much more effective cross-weave material.

This study investigated the fiber volume fraction effects on the fatigue life of a unidirectional SCS-6/Ti-15-3 laminate. It provided fatigue life data for TMC's under the fully-reversed, strain-controlled mode at elevated temperature. However, more testing of

this TMC is required to completely understand the fatigue response. Expanded maximum strain ranges that account for fatigue beyond 100,000 cycles are needed for practical application of the different  $V_f$  material. This would lead to the expansion of the  $\epsilon$ -N diagram to determine the fatigue limit of the composite. Because of the cost of the material and testing time, only a few tests could be repeated in this study. Further research examining the statistical scatter of fatigue life with a high confidence would also, therefore, be extremely helpful to future researchers.

## Bibliography

1. Bartolotta, P., Brindley, P., "High Temperature Fatigue Behavior of a SiC/Ti-24Al-11Nb Composite," NASA Technical Memorandum 103157, 1990.
2. Boyum, E., Investigation of Tension-Compression Fatigue Behavior of a Cross-Ply MMC at Room and Elevated Temperature, MS Thesis, AFIT/GAE/ENY/93D-6. School of Engineering, Air Force Institute of Technology (AETC), Wright-Patterson AFB, Ohio, December 1993.
3. Calcaterra, J.R., Mall, S., and Coghlan, S.C., "Degradation of Residual Strength in SCS-6/Ti-15-3 Due to Fully-Reversed Fatigue," Submitted to TMS Fall Meeting, Indianapolis, IN, September 14-18, 1997. Paper will be presented in a special issue of Metallurgical and Materials Transactions, subject to peer review.
4. Calcaterra, J., Mall, S., Coghlan, S., "Fiber Volume Fraction Effects of the Strain-Controlled Fatigue of SiC/Ti-15-3," NASA Conference Publication 10192, Vol. 2: Advanced Alloys and MMC's, Paper 32, 1997.
5. Castelli, M. and J. Gayda. "An Overview of Elevated Temperature Damage Mechanisms and Fatigue Behavior of a Unidirectional SiC/Ti-15-3 Composite," DE-Vol. 55, Reliability, Stress Analysis, and Failure Prevention, ASME, 1993, pp. 213-221.
6. Castelli, M., Ellis, J., Bartolotta, P., "Thermomechanical Testing Techniques for High Temperature Composites: TMF Behavior of SiC/Ti-15-3," NASA Technical Memorandum 103171, 1990.
7. Covey, S., Lerch, B., and Jayaraman, N., "Fiber Volume Fraction Effects on Fatigue Crack Growth in SiC/Ti-15-3 Composite," Materials Science & Engineering, A200, 1995, pp.68-77.
8. Dennis, L., Fatigue Behavior of a Cross-Ply Metal Matrix Composite at Elevated Temperature Under Strain-Controlled Mode. MS Thesis, AFIT/GAE/ENY/94D-7. School of Engineering, Air Force Institute of Technology (AETC), Wright-Patterson AFB, OH, December 1994.
9. Gabb, T., Gayda, J., Lerch, B., Halford, G., "The Effect of Matrix Mechanical Properties on [0]<sub>g</sub> Unidirectional SiC/Ti-15-3 Composite Fatigue Resistance," Scripta Metallurgica et Materialia, Vol. 25, 1991, pp. 2879-2884.



10. Gabb, T., J. Gayda and R. MacKay. "Isothermal and Nonisothermal Fatigue Behavior of a Metal Matrix Composite." Journal of Composites and Materials, Vol. 24, June 1990, pp. 667-686.
11. Gayda, J., et al., "The Isothermal Fatigue Behavior of a Unidirectional SiC/Ti Composite and the Ti Alloy Matrix," NASA Technical Memorandum 101984, 1989.
12. Gayda, J. and T. Gabb. "Effect of Heating Mode and Specimen Geometry on Fatigue Properties of a MMC," NASA Conference Publication, Paper 31, 1990.
13. Gayda, J. and T. Gabb. "The Effect of Fiber Content on the Fatigue Life of SCS-6/Ti-15-3 Composite," Scripta Metallurgica et Materialia, Vol. 30, 1994, pp. 469-474.
14. Jackson, S., Stress/Strain Ratio Effects on Fatigue Response of a SCS-6/Ti-15-3 Metal Matrix Composite at Elevated Temperature. MS Thesis, AFIT/GAE/ENY/95D-14. School of Engineering, Air Force Institute of Technology (AETC), Wright-Patterson AFB, OH, Dec. 1990.
15. Johnson, S., S. Lubowinski and A. Highsmith, "Mechanical Characterization of Unnotched SiC/Ti-15-3 Metal Matrix Composites at Room Temperature." Thermal and Mechanical Behavior of Metal Matrix and Ceramic Matrix Composites, ASTM STP 1080. J.M. Kennedy, H.H. Moeller, and W.S. Johnson, Eds., ASTM, Philadelphia, 1990, pp. 193-218.
16. Konitzer, D., and M. Loretto, "Interfacial Interactions in Titanium-based Metal Matrix Composites," Interfacial Phenomena in Composites: Processing, Characterization and Mechanical Properties, Suresh, S. and A. Needleman Eds., Elsevier Applied Science: New York, 1989.
17. Kraabel, D., Investigation of Tension-Compression Fatigue Behavior of a Unidirectional Metal Matrix Composite at Elevated Temperature, MS Thesis, AFIT/GAE/ENY/94D-16, School of Engineering, Air Force Institute of Technology (AETC), Wright-Patterson AFB, OH, December 1994.
18. Lerch, B., Halford, G., "Effects of Control Mode and R-ratio on the Fatigue Behavior of a MMC," Materials Science and Engineering, A200, 1995, pp. 47-54.
19. Lerch, B., and J. Saltsman. "Tensile Deformation Damage in SiC Reinforced Ti-15V-3Cr-3Al-3Sn." NASA Technical Memorandum 103620, April 1991.

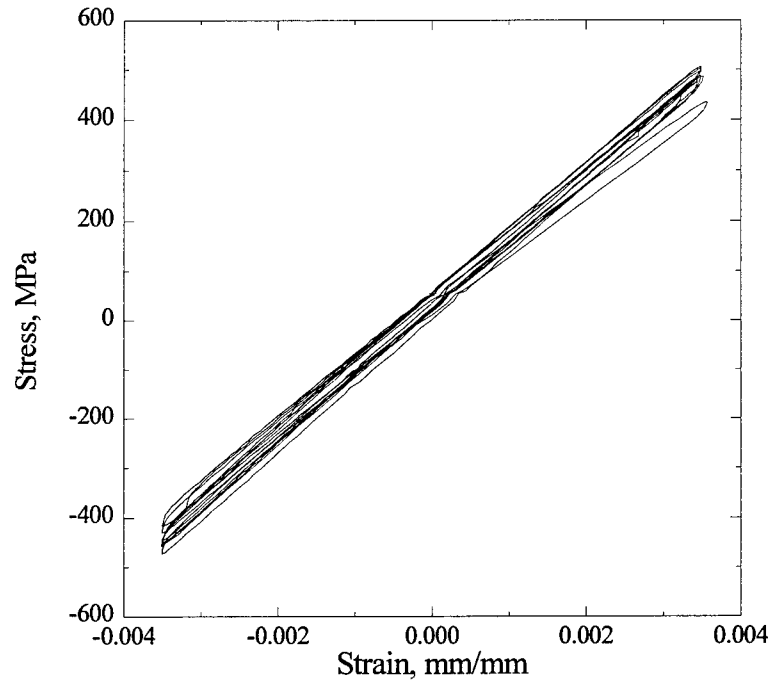
20. MacKay, R., "Effect of Fiber Spacing on Interfacial Damage in a Metal Matrix Composite," Scripta Metallurgica et Materialia, Vol. 24, 1990, pp. 167.
21. Majumdar, B. and G. Newaz. "In-Phase Thermomechanical Fatigue of Metal Matrix Composites: Deformation Response and Progressive Damage Mechanisms," Composite Materials: Testing and Design, ASTM STP 1274. ASTM, Philadelphia, 1996, pp. 264.
22. Majumdar, B. and G. Newaz. "Inelastic Fatigue of Metal Matrix Composites: Compression and Fatigue." Submitted for publication. Batelle Memorial Institute, Columbus, OH.
23. Majumdar, B. and G. Newaz. "Mechanisms of Fatigue Damage and Failure of a SCS-6/Ti-15-3 Composite." Mechanisms and Mechanics of Composite Fracture, ASTM Proceedings, October 1993.
24. Majumdar, B. and G. Newaz. "Isothermal Fatigue Mechanisms in Ti-based Metal Matrix Composites," NASA Contractor Report 191181, 1993.
25. Mallick, P.K., Fiber-Reinforced Composites, New York: Marcel Dekker, Inc. 1993.
26. Naik, R., W. Pollock and W.S. Johnson. "Effect of a High-Temperature Cycle on the Mechanical Properties of Silicon Carbide/Titanium Metal Matrix Composite," Journal of Materials Science, 26, 1991, pp. 2913-2920.
27. Nicholas, T. and Ahmad, J., "Modeling Fiber Breakage in a Metal Matrix Composite," Composites Science and Technology, 52, 1994, pp.29-38.
28. Pollock, W. and W. S. Johnson. "Characterization of Unnotched SiC/Ti-15-3 Metal Matrix Composites at 650°C," NASA Technical Memorandum 102699, NASA Langley Research Center, September 1990.
29. Robertson, D., "User's Manual for the Laminated Composite Inelastic Solver Computer Program," AFIT/ENY/TR96-01, Air Force Institute of Technology (AETC), Wright-Patterson AFB, OH, 1996.
30. Sanders, B., Characterization of Fatigue Damage in a Metal Matrix Composite (SCS-6/Ti-15-3) at Elevated Temperature, PhD Dissertation, AFIT/DS/AA/93-4,

School of Engineering, Air Force Institute of Technology (AETC), Wright-Patterson AFB, OH, December 1993.

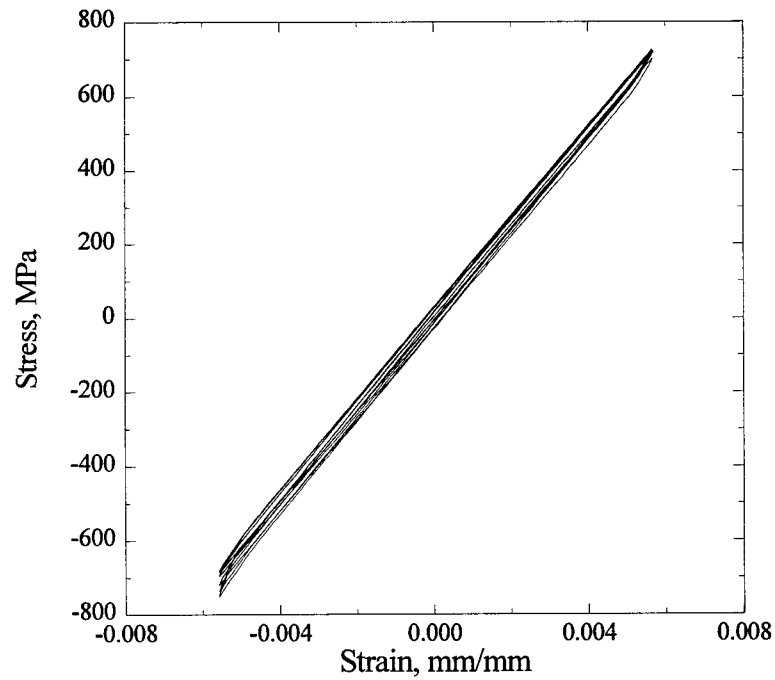
31. Talreja, R., Fatigue of Composite Materials, Lancaster: Technomic Publishing Company, 1987.

## Appendix

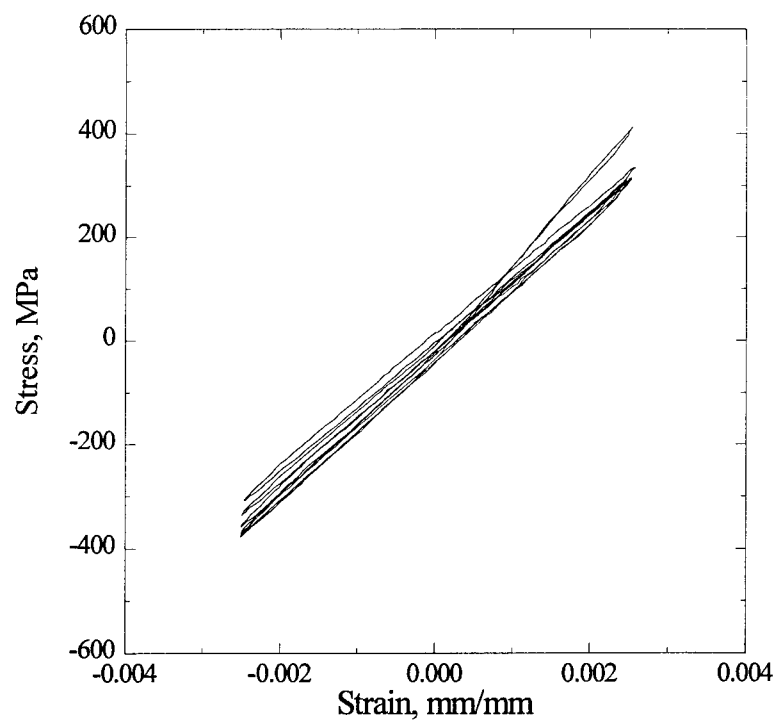
### Stress-Strain Curves



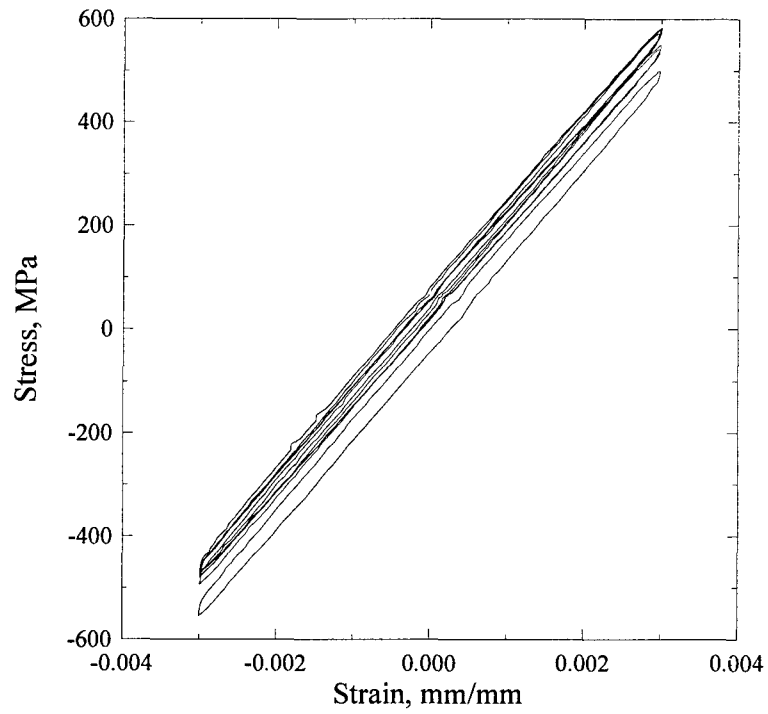
### Stress-Strain Loops for 15% $V_p$ 0.35% Maximum Strain Test



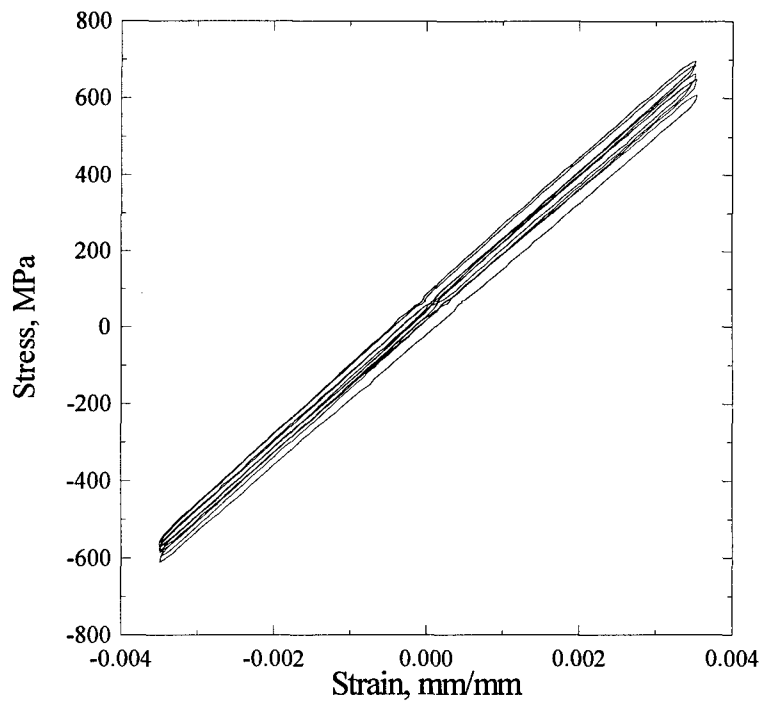
### Stress-Strain Loops for 15% $V_p$ 0.55% Maximum Strain Test



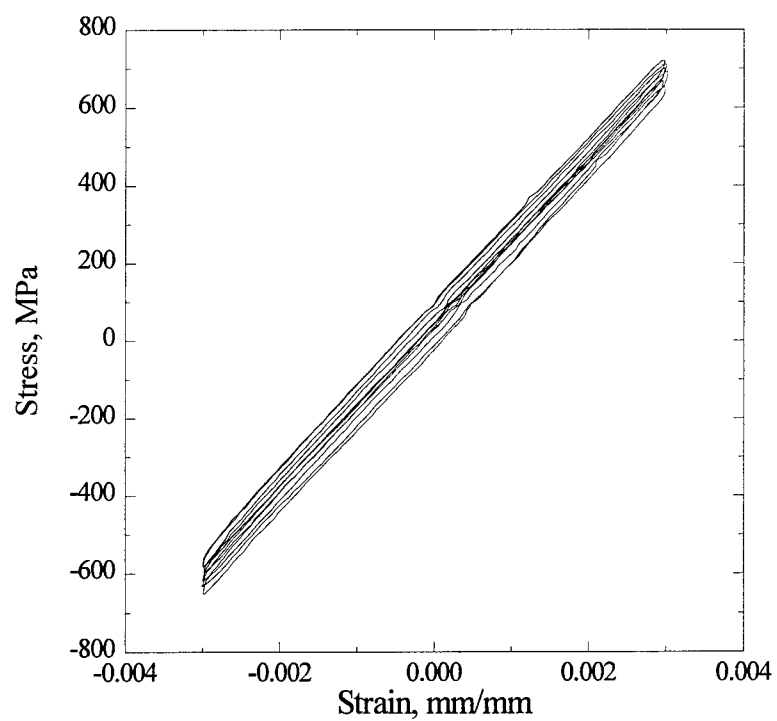
**Stress-Strain Loops for 15%  $V_p$ , 0.25% Maximum Strain Test**



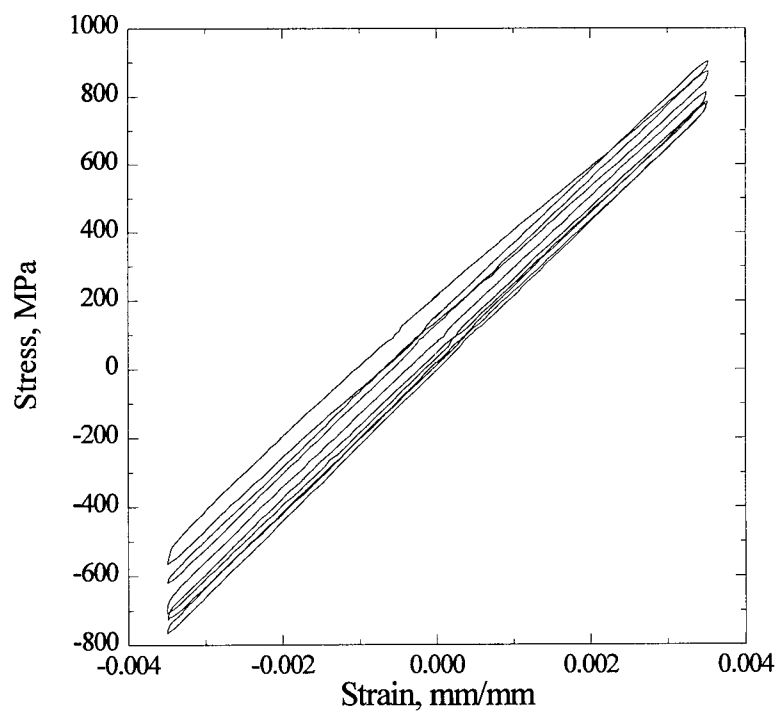
**Stress-Strain Loops for 25%  $V_p$  0.30% Maximum Strain Test**



**Stress-Strain Loops for 25%  $V_p$  0.35% Maximum Strain Test**



**Stress-Strain Loops for 42%  $V_p$  0.30% Maximum Strain Test**



**Stress-Strain Loops for 42%  $V_p$  0.35% Maximum Strain Test**

## Vita

Sean C. Coghlan [REDACTED] graduated from Olentangy High School, Delaware, Ohio in 1991. He entered the University of Dayton, Dayton, Ohio later that year. In May of 1995 he graduated with a Bachelor of Science in Mechanical Engineering with a concentration in aerospace. That summer he was awarded a full scholarship from the Dayton Area Graduate Studies Institute and entered the School of Engineering at the Air Force Institute of Technology, Wright Patterson AFB, Ohio in October 1995.



# REPORT DOCUMENTATION PAGE

Form Approved

OMB No. 0704-0188

Public reporting burden for this collection of information is estimated to average 1 hour per response, including the time for reviewing instructions, searching existing data sources, gathering and maintaining the data needed, and completing and reviewing the collection of information. Send comments regarding this burden estimate or any other aspect of this collection of information, including suggestions for reducing this burden, to Washington Headquarters Services, Directorate for Information Operations and Reports, 1215 Jefferson Davis Highway, Suite 1204, Arlington, VA 22202-4302, and to the Office of Management and Budget, Paperwork Reduction Project (0704-0188), Washington, DC 20503

1. AGENCY USE ONLY (Leave blank)		2. REPORT DATE September 1997		3. REPORT TYPE AND DATES COVERED Master's Thesis	
4. TITLE AND SUBTITLE Fiber Volume Fraction Effect on the Fatigue Response of a SCS-6/Ti-15-3 Metal Matrix Composite at Elevated Temperature				5. FUNDING NUMBERS	
6. AUTHOR(S) Sean C. Coghlan, DAGSI					
7. PERFORMING ORGANIZATION NAME(S) AND ADDRESS(ES) AFIT/ENY, BLDG 640 2950 P STREET WRIGHT-PATTERSON AFB, OH 45433-6583				8. PERFORMING ORGANIZATION REPORT NUMBER AFIT/GAE/ENY/97S-01	
9. SPONSORING/MONITORING AGENCY NAME(S) AND ADDRESS(ES) Ted Fecke WL/POTC 2130 Eighth St. Ste. 1 WPAFB, OH 45433-7542				10. SPONSORING/MONITORING AGENCY REPORT NUMBER	
11. SUPPLEMENTARY NOTES					
12a. DISTRIBUTION/AVAILABILITY STATEMENT Approved for public release; distribution unlimited				12b. DISTRIBUTION CODE A	
13. ABSTRACT (Maximum 200 words)  An investigation into the fatigue behavior of unidirectional SCS-6/Ti-15-3 fiber reinforced metal matrix composite was conducted. Three different fiber volume fractions of 15%, 25%, and 42% were studied. Tests were conducted under fully-reversed, strain-controlled conditions at a temperature of 427°C. Matrix fatigue crack initiation and propagation was observed to be the dominant damage mechanism. A molybdenum cross-weave used in the 15% and 42% fiber volume fraction material was found to be detrimental to fatigue life. At applied strain ranges at or above 0.8%, fatigue life was similar among all fiber volume fractions. Below the 0.8% strain range, there was an increasing fatigue life with increasing fiber volume fraction. The higher fiber volume fraction material had a longer fatigue life than the low fiber volume fraction material at lower applied strain ranges.					
14. SUBJECT TERMS Metal Matrix Composites, Strain Control, Fatigue, Fiber Volume Fraction, Tension-Compression, Elevated Temperature				15. NUMBER OF PAGES 58	
				16. PRICE CODE	
17. SECURITY CLASSIFICATION OF REPORT Unclassified	18. SECURITY CLASSIFICATION OF THIS PAGE Unclassified	19. SECURITY CLASSIFICATION OF ABSTRACT Unclassified	20. LIMITATION OF ABSTRACT UL		